Nonlinear characteristics of a multi-degree-of-freedom wind turbine's gear transmission system involving friction

Qiang Zhang
Wuhan University
Xiaosun Wang (wxs@whu.edu.cn)
Wuhan University
Shaobo Cheng
Wuhan University
Fuqi Xie
Wuhan University
Shijing Wu
Wuhan University

Research Article

Keywords: Compound gear transmission system(CGTS), time-varying meshing friction(TVMF), time-varying meshing stiffness (TMVS), mixed elastohydrodynamic lubrication (MEHL), nonlinear dynamic characteristic

Posted Date: August 17th, 2021

DOI: https://doi.org/10.21203/rs.3.rs-782807/v1

Version of Record: A version of this preprint was published at Nonlinear Dynamics on January 17th, 2022. See the published version at https://doi.org/10.1007/s11071-021-07092-w.

Nonlinear characteristics of a multi-degree-of-freedom wind turbine's gear transmission system involving friction

Qiang Zhang[a], Xiaosun Wang[*], Shaobo Cheng, Fuqi Xie, Shijing Wu

[a]*Department of Mechanical Engineering, School of Power and Mechanical Engineering, Wuhan University, Wuhan, 430072, P.R.China*

Abstract

In this study, a 42-degree-of-freedom (42-DOF) translation-torsion coupling dynamics model of the wind turbine's compound gear transmission system considering time-varying meshing friction, time-varying meshing stiffness, meshing damping, meshing error and backlash is proposed. Considering the different meshing between internal and external teeth of planetary gear, the time-varying meshing stiffness is calculated by using the cantilever beam theory. An improved mesh friction model takes account into the mixing of elastohydrodynamic lubrication (EHL) and boundary lubrication to calculate the time-varying mesh friction. The bifurcation diagram is used to analyze the bifurcation and chaos characteristics of the system under the excitation frequency as bifurcation parameter. Meanwhile, the dynamic characteristics of the gear system are identified from the time domain diagrams, phase diagrams, Poincare maps and amplitude-frequency spectrums of the gear system. The results show that the system has complex bifurcation and chaotic behaviors including periodic, quasi-periodic, chaotic motion. The bifurcation characteristics of the system become complicated and the chaotic region increases considering the effects of friction in the high frequency region.

Keywords: Compound gear transmission system(CGTS), time-varying meshing friction(TVMF), time-varying meshing stiffness (TMVS), mixed elastohydrodynamic lubrication (MEHL), nonlinear dynamic characteristic.

1. Introduction

Compound gear transmission system is one of the most important transmission device in wind turbine. Due to harsh operation environment, multi-aspect excitations and complicated structure, wind turbine's compound gear transmission system is considered vulnerable in most cases. Thus, it is necessary to study the nonlinear dynamic characteristics of wind turbine's compound gear transmission system and evolution mechanism by establishing reliable dynamic model of compound gear transmission system to ensure the safe and stable operation for wind turbine's compound gear transmission system.

A number of research studies have been conducted on the dynamics modeling of planetary gear systems[1]. Ambarisha and parker[2,3] adopts analytical model and finite element model to study the nonlinear dynamics of planetary gear, and proposes a lumped parameter analytical model. By comparing with the finite element results in the complex nonlinear dynamics range in the system, the validity of the model is verified. Zhou et al.[4]established multi-degree-of-freedom dynamic model considering the coupling lateral-torsional vibration. and the coupled multi-body dynamics of the spur gear rotor bearing system was studied containing backlash,

[*]wxs@whu.edu.cn

transmission error, eccentricity, gravity. The dynamic behaviors were investigated in different system parameters. Wang et al.[5] established the planetary gear transmission system considering the coupling effects of multiple nonlinear factors. The Runge-Kutta numerical method is used to solve the system vibration equation. Wang et al.[6] established 8-DOF gear system and applied improved meshing stiffness model to calculate the time-varying meshing stiffness. The dynamic chaos and bifurcation behavior of translational - torsional coupled system are analyzed. Zhu et al.[7] studied the influence of backlash on the shell differential planetary gear system. The results show that the backlash will cause the bilateral impact of the meshing tooth, resulting in chaotic motion of the system. The change of backlash at any transmission stage has a significant effect on gear meshing force and dynamic characteristics of the system. It can be seen from the above literatures that the research on the nonlinear dynamic characteristics of planetary gear transmission system mainly focuses on the dynamic response analysis of single-stage planetary gear transmission system. Few studies have been done on two-stage planetary gear system, especially the two-stage planetary gear coupling translation-torsion system of wind turbine's compound gear transmission system.

During operation of compound planetary gear transmission system, friction is a strongly nonlinear internal excitation,which is positively correlated with the dynamic characteristics of compound gear transmission system. He et al.[8-9]proposed a new method to consider the sliding friction and time-varying meshing stiffness into the analysis model of spur gear, and studied the influence of its dynamic characteristics. Kahraman et al[10-13] proposed a tribo-dynamics model for spur gear pairs. The iterative calculation scheme of lubrication and dynamic model is proposed to make the tribological and dynamic behavior of spur gear pair fully coupled. Huaiju Liu et al.[14,15] proposed a single-stage spur gear modle considering starved lubrication. By studying the dynamic coupling relationship between friction dynamics and gear system, the dynamic meshing force of the system is predicted. A calculation method of meshing stiffness under starved lubrication is provided. The research of gear lubrication dynamics mainly focuses on single pair of meshing gears. Hou et al.[16] proposed to solve the different friction tooth surfaces of single stage gear by subsection, and then the friction force and friction torque are analyzed by summation. Han et al.[17] investigated the dynamic response of a pair of helical gears considering the interaction between friction and time-varying meshing stiffness, and analyzed the influence of friction on the dynamic characteristics of the system. Yi et al.[18] established a fractal contact model suitable for gear pair contact considering the influence of roughness on the normal contact stiffness of gear, and analyzed the influence of roughness on the dynamic characteristics of the system. Lin et al.[19] established a nonlinear dynamic model of gear considering time-varying meshing stiffness, backlash, sliding friction and random external load. The results show that under the condition of deterministic load, friction makes the duration of the system in the stable state longer and the periodic stability of the system better. Li et al.[20] obtained time-varying meshing friction coefficient of tooth surface obtained by fitting the experimental results of double disks. Chen et al.[21] studied the calculation method of friction coefficient and meshing efficiency of plastic wire gear pair under dry friction condition, the dynamic characteristics of the system under dry friction condition are obtained. Bae et al.[22] adopts finite element simulation method to the contact stress between coated polymer gears considering different friction coefficients. Keller et al.[23] established a thermal elastohydrodynamic model for the single tooth gear. the method is provided to remove the Hertz deformation of macro-deformation tooth profile. Park et al.[24] investigated friction and Transmission error of spur gear due to sliding friction under quasi-static condition. Ma et al.[25] proposed an improved analytical model for time-varying meshing stiffness calculation considering friction between teeth surfaces. Ghosh Chakraborty[26] studied a 6-DOF translation-rotation model considering friction. The influence of different friction parameters on the system is analyzed.

It can be seen from the above studies that the research model for multi-degree-of-freedom planetary gear is mainly the purely rotational of gear system. The study of gear friction is mostly based on single pair

gear. There exists close coupling relationship between the translational and torsional vibrations of gear system. The motivation of this paper is to established multi-degree-of-freedom translation-torsion coupling dynamics planetary gear model to accurately describe the dynamic behavior of wind turbine's compound gear transmission system. The consideration of TVMS is implemented by the cantilever beam theory. Another main research content is the calculation of time-varying meshing friction (TVMF). In this paper, a 42-DOF translation-torsion coupling dynamics model of the wind turbine's gear transmission system considering TVMF, TVMS, meshing damping, meshing error and backlash is established. The system dimensionless equation is solved by Runge-Kutta numerical method. The dynamic characteristics of the gear system are identified from the bifurcation diagram, time domain diagrams, phase diagrams, Poincare maps and amplitude-frequency spectrums of the gear system. The research can provide some useful information for the operation of wind turbine's gear transmission system.

2. Dynamic modelling of gear system

Taking the time-varying meshing friction and time-varying meshing stiffness into account, a 42-DOF translation-torsion coupling lumped parameter dynamics model is established, as shown in Fig. 1. Fig. 1(a) presents wind turbine gear's transmission system consists of two planetary gear transmission operating at the low-speed stage and intermediate stage and one fixed-axis gear transmissions operating at the high-speed stage, respectively, which have large transmission ratio in relatively compact structures. The parameters of the planetary gear transmission system (I and II) is shown in Fig.1(b). In this model, the meshing tooth surfaces of involute spur gears are simplified as spring-damping system. The planetary gear transmission system consists components such as carrier (c), ring (r), sun (s), planet (p_n(n=1,2,...,N)). The stiffness of springs k_{st}, k_{rt}, k_{ct} can be defined according to the power distribution of the system. Each spur gears $i(i = s, r, c, p_n(n = 1, 2, ..., N))$ is simplified as a rigid disc of base radius r_i, mass moment of inertia I_i, and angular displacement θ_i. The torsional displacements are represented by u_c, u_r, u_s, u_{P_n}, respectively. Fig. 1(c) shows the translation-torsion coupling dynamics model of the fixed-axis gear system including the gear(g_1) and pinion(g_2). The carrier (c_1) and the pinion(g_2) are identified as input(T_{c_1}) and output(T_{g_2}) components of the system. Two coordinates (OXY, oxy) are created in an effort to establish the dynamic equations of the system easily. The center of the fixed coordinate system (OXY) is located in the center of the sun gear. The motion coordinate system (oxy) is fixed with the planetary carrier and rotates with its theoretical angular velocity (ω_c). The relationship between the two coordinates system is shown in Fig.1(b). In terms of the analysis above, the relationship could be obtained as follows,

$$\begin{cases} x = X\cos\omega_c t + Y\sin\omega_c t \\ y = -X\sin\omega_c t + Y\cos\omega_c t \end{cases} \tag{1}$$

Then, the absolute velocity can be represented in the rotational coordinate system as follows,

$$\begin{cases} \dot{X} = (\dot{x} - \omega_c y)\cos\omega_c t - (\dot{y} + \omega_c x)\sin\omega_c t \\ \dot{Y} = (\dot{y} + \omega_c x)\cos\omega_c t + (\dot{x} - \omega_c y)\sin\omega_c t \end{cases} \tag{2}$$

2.1. Equivalent displacements

Define θ_i $(i = s_1, r_1, c_1, p_{1,n}(n = 1, 2, ..., N), g_1, s_2, r_2, c_2, p_{2,n}(n = 1, 2, ..., N), g_1, g_2)$ as the angular displacement of each gear body, which is measured in the fixed coordinate system OXY. So the equivalent gear meshing displacements u_i in the meshing line direction are defines as

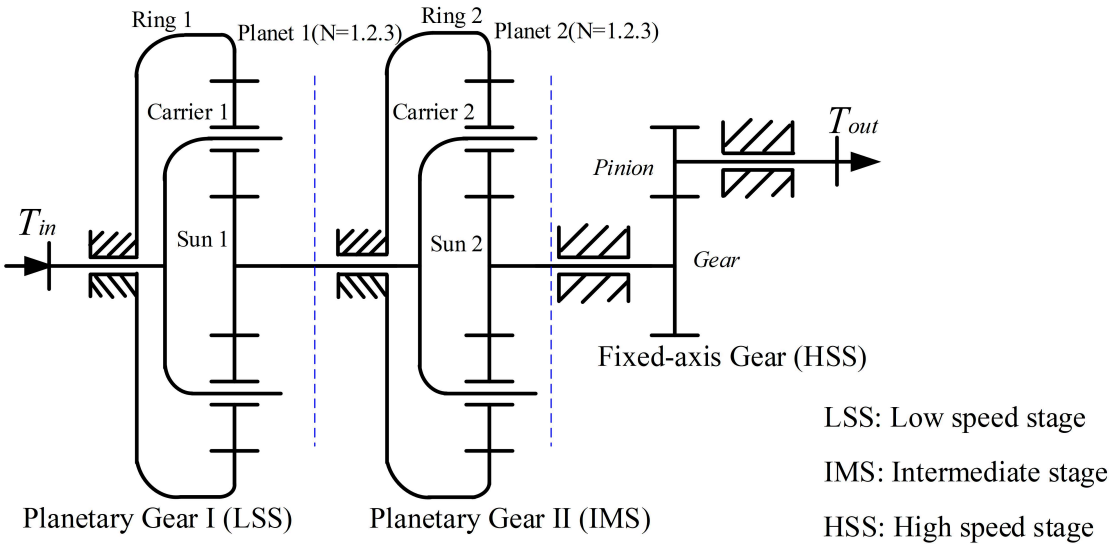

a. Typical drivetrain configuration for a wind turbine

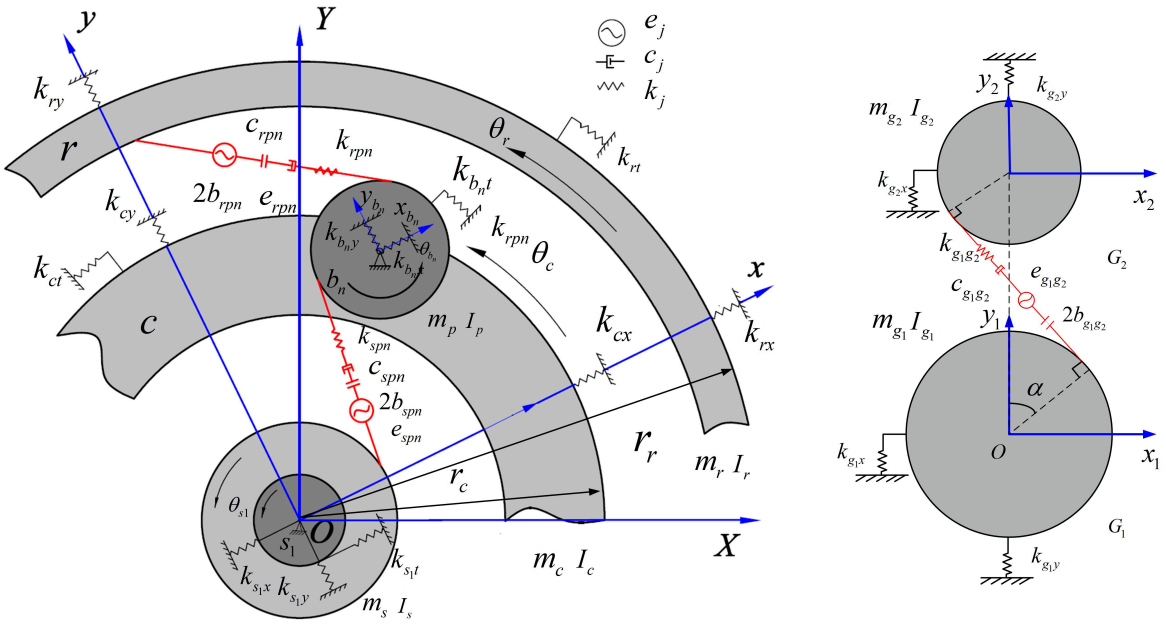

b. Dynamic model of planetary Gearbox I or II c. Dynamic model of Fixed-axis Gearbox

Fig. 1. The dynamic model of the wind turbine's gear system

$$\begin{cases} u_{s_1} = r_{p_{1,n}s_1}\theta_{s_1}, u_{r_1} = r_{p_{1,n}r_1}\theta_{r_1}, u_{c_1} = r_{p_{1,n}c_1}\theta_{c_1}, u_{p_{1,n}} = r_{p_{i,n}}\theta_{p_{1,n}} \\ u_{s_2} = r_{p_{2,n}s_2}\theta_{s_2}, u_{r_2} = r_{p_{2,n}r_2}\theta_{r_2}, u_{c_2} = r_{p_{2,n}c_2}\theta_{c_2}, u_{p_{2,n}} = r_{p_{2,n}}\theta_{p_{2,n}} \\ u_{g_1} = r_{g_1}\theta_{g_1}, u_{g_2} = r_{g_2}\theta_{g_2} \end{cases} \tag{3}$$

In order to ensure the contact of teeth surface on meshing performance, it is assumed that the relative deformation of gears is completely changed into elastic deformation on teeth surface along with the meshing line-direction. According to the geometrical relationships, the relative gear mesh displacements $\delta_j (j = s_1p_{1,n}, r_1p_{1,n}, s_2p_{2,n}, r_2p_{2,n}, c_2p_{2,n}, g_1g_2, (n = 1, 2, ..., N))$ in the rotational coordinate system, and the line displacements $\delta_j (j = c_1p_{1,n}, c_2p_{2,n})$ of planet gears relative to the planet carrier on the x-axis and y-axis of the planet carrier can be represented as,

$$\begin{cases} \delta_{s_1p_{1,n}} = (x_{p_{1,n}} - x_{s_1})\sin(\varphi_{s_1p_{1,n}}) + (y_{s_1} - y_{p_{1,n}})\cos(\varphi_{s_1p_{1,n}}) + u_{s_1} + u_{p_{1,n}} - u_c\frac{r_{s_1}+r_{p_{1,n}}}{r_{c_1}} - E_{s_1p_{1,n}} \\ \delta_{r_1p_{1,n}} = (x_{p_{1,n}} - x_{r_1})\sin(\varphi_{r_1p_{1,n}}) + (y_{r_1} - y_{p_{1,n}})\cos(\varphi_{r_1p_{1,n}}) + u_{r_1} - u_{p_{1,n}} - u_{c_1}\frac{r_{s_1}+r_{p_{1,n}}}{r_{c_1}} - E_{r_1p_{1,n}} \\ \delta_{c_1p_{1,n}x} = x_{p_{1,n}} - x_{c_1} \\ \delta_{c_1p_{1,n}y} = x_{p_{1,n}} - x_{c_1} \\ \delta_{s_2p_{2,n}} = (x_{p_{2,n}} - x_{s_2})\sin(\varphi_{s_2p_{2,n}}) + (y_{s_2} - y_{p_{2,n}})\cos(\varphi_{s_2p_{2,n}}) + u_{s_2} + u_{p_{2,n}} - u_c\frac{r_{s_2}+r_{p_{2,n}}}{r_{c_2}} - E_{s_2p_{2,n}} \\ \delta_{r_2p_{2,n}} = (x_{p_{2,n}} - x_{r_2})\sin(\varphi_{r_2p_{2,n}}) + (y_{r_2} - y_{p_{2,n}})\cos(\varphi_{r_2p_{2,n}}) + u_{r_2} - u_{p_{2,n}} - u_{c_2}\frac{r_{s_2}+r_{p_{2,n}}}{r_{c_2}} - E_{r_2p_{2,n}} \\ \delta_{c_2p_{2,n}x} = x_{p_{2,n}} - x_{c_2} \\ \delta_{c_2p_{2,n}y} = x_{p_{2,n}} - x_{c_2} \\ \delta_{g_1g_2} = u_{g_1} + u_{g_2} - E_{g_1g_2} \end{cases} \tag{4}$$

where E_j are the transmission errors, and φ_j is the relative engagement angle.

The vibration of the system is mainly caused by errors existing inevitably during the manufacturing and assembly process. The position of the planet gear is changed as a function of gear position error. O_{P_n} is the ideal location of center of the planet gear. The gear position error of magnitude A_{P_n} makes the ideal location point O_{P_n} move to O'_{P_n}. The tangential magnitude of the position error of planet gear can be expressed as,

$$\begin{cases} \bar{A}_{p_{1,n}-s_1p_{1,n}} = -A_{p_{1,n}}\sin(\alpha_{s_1} + \varphi_{p_{1,n}}) \\ \bar{A}_{p_{1,n}-r_1p_{1,n}} = -A_{p_{1,n}}\sin(\varphi_{p_{1,n}} - \alpha_{r_1}) \\ \bar{A}_{p_{2,n}-s_2p_{2,n}} = -A_{p_{2,n}}\sin(\alpha_{s_2} + \varphi_{p_{2,n}}) \\ \bar{A}_{p_{2,n}-r_2p_{2,n}} = -A_{p_{2,n}}\sin(\varphi_{p_{2,n}} - \alpha_{r_2}) \end{cases} \tag{5}$$

where α_s, α_r, φ_{p_n} are the pressure angle of the sun gear, the pressure angle of the ring gear and the initial angle of position error and the planet spacing angles, respectively.

Similarly, the run-out error on the reference circle of the gear can be expressed as,

$$\begin{cases} \bar{e}_{s_1-s_1p_{1,n}} = e_{s_1}\sin((\omega_{s_1} - \omega_{c_1})t + \alpha_{s_1} + \varphi_{es_1} - \varphi_{p_{1,n}}) \\ \bar{e}_{p_{1,n}-s_1p_{1,n}} = -e_{p_{1,n}}\sin((\omega_{p_{1,n}} - \omega_{c_1})t + \alpha_{s_1} + \varphi_{ep_{1,n}}) \\ \bar{e}_{p_{1,n}-r_1p_{1,n}} = -e_{p_{1,n}}\sin((\omega_{p_{1,n}} - \omega_{c_1})t + \varphi_{ep_{1,n}} - \alpha_{r_1}) \\ \bar{e}_{r_1-r_1p_{1,n}} = e_{r_1}\sin((\omega_{r_1} - \omega_{c_1})t + \alpha_{r_1} + \varphi_{er_1} - \varphi_{p_{1,n}}) \end{cases} \tag{6}$$

where ω_i, φ_{ei}, φ_{p_n} are the theoretical angular velocity of the component, the initial angle of the run-out error on the reference circle and the planet spacing angles, respectively. here, $\varphi_{p_n} = 2\pi\frac{n-1}{N}$. The transmission errors on the line of action can be represented as,

$$\begin{cases} E_{s_1p_n} = \bar{A}_{p_n-s_1p_n} + \bar{e}_{s_1-s_1p_n} + \bar{e}_{p_n-s_1p_n} \\ E_{r_1p_n} = \bar{A}_{p_n-r_1p_n} + \bar{e}_{r_1-r_{p_n}} + \bar{e}_{p_n-r_1p_n} \\ E_{s_2p_{2n}} = \bar{A}_{p_{2n}-s_2p_{2n}} + \bar{e}_{s_2-s_2p_{2n}} + \bar{e}_{p_{2n}-s_2p_{2n}} \\ E_{r_2p_{2n}} = \bar{A}_{p_{2n}-r_2p_{2n}} + \bar{e}_{r_2-r_2p_{2n}} + \bar{e}_{p_{2n}-r_2p_{2n}} \end{cases} \tag{7}$$

The gear backlash exists in the meshing gear teeth due to the need of lubrication, the errors caused by manufacturing and installing, and the wear during operation. And the piecewise-linear backlash functions $f(\delta_j)$ can be defined as,

$$f(\delta_j) = \begin{cases} \delta_j - b_j & \delta_j > b_j \\ 0 & |\delta_j| \le b_j \\ \delta_j + b_j & \delta_j < -b_j \end{cases} \tag{8}$$

where b_j is the gear backlash, and δ_j is the relative gear mesh displacement. The dimension tolerance must be considered that the translational vibration is taken into consideration for the components. The radial support force f_{xi} and f_{yi} are changed because of the radial clearance (Δb) caused by dimension tolerance of the shaft and the hole. The principle of the relationship between the force and the clearance which can be expressed as,

$$\begin{cases} f_{xi} = \gamma_i k_i \delta_{xi} \\ f_{yi} = \gamma_i k_i \delta_{yi} \end{cases} \tag{9}$$

where k_i,δ_{xi}, δ_{yi} are the radial support stiffness and radial vibrational displacement. And γ_i determines whether the shaft and the hole are in contact, according to,

$$\gamma_i = \begin{cases} 1 - \frac{\Delta b}{\sqrt{\delta_{xi}^2+\delta_{yi}^2}} & \Delta b < \sqrt{\delta_{xi}^2 + \delta_{yi}^2} \\ 0 & \Delta b \ge \sqrt{\delta_{xi}^2 + \delta_{yi}^2} \end{cases} \tag{10}$$

2.2. System differential equation of motion

The general coordinate q is introduced in order to establish the motion differential equations of the gear system.

$$q = \left\{ \begin{array}{l} x_{s_1}, y_{s_1}, \theta_{s_1}, x_{c_1}, y_{c_1}, \theta_{c_1}, x_{r_1}, y_{r_1}, \theta_{r_1}, x_{p_{1,n}}, y_{p_{1,n}}, \theta_{p_{1,n}}, x_{s_2}, y_{s_2}, \theta_{s_2}, \\ x_{c_2}, y_{c_2}, \theta_{c_2}, x_{r_2}, y_{r_2}, \theta_{r_2}, x_{p_{2,n}}, y_{p_{2,n}}, \theta_{p_{2,n}}, x_{g_1}, y_{g_1}, \theta_{g_1}, x_{g_2}, y_{g_2}, \theta_{g_2} \end{array} \right\}^T \tag{11}$$

Lagrange function of planetary transmission system(L_1), fixed-axis transmissions(L_2) and coupling relations between levels(L_3) are expressed as,

$$
\begin{cases}
L_1 = \frac{1}{2}I_{s_i}\dot{\theta}_{s_i}^2 + \frac{1}{2}I_{c_i}\dot{\theta}_{c_i}^2 + \frac{1}{2}I_{r_i}\dot{\theta}_{r_i}^2 + \frac{1}{2}\sum_{n=1}^{N}[m_p \cdot (r_s + r_p)^2 \cdot \dot{\theta}_c^2 + I_{p_n}\dot{\theta}_{p_n}^2] \\
+ \frac{1}{2}m_{s_i} \cdot (\dot{X}_{s_i}^2 + \dot{Y}_{s_i}^2) + \frac{1}{2}m_{c_i} \cdot (\dot{X}_{c_i}^2 + \dot{Y}_{c_i}^2) + \frac{1}{2}m_{r_i} \cdot (\dot{X}_{r_i}^2 + \dot{Y}_{r_i}^2) + \frac{1}{2}\sum_{n=1}^{N} m_{p_i} \cdot (\dot{X}_{p_i}^2 + \dot{Y}_{p_i}^2) \\
- \frac{1}{2}\sum_{n=1}^{N} k_{s_i p_{i,n}} \cdot \delta_{s_i p_{i,n}}^2 - \frac{1}{2}\sum_{n=1}^{N} k_{c_i p_{i,n}} \cdot (\delta_{p_{i,n} c_i x}^2 + \delta_{p_{i,n} c_i y}^2) - \frac{1}{2}\sum_{n=1}^{N} k_{r_i p_{i,n}} \cdot \delta_{r_i p_{i,n}}^2 \\
- \frac{1}{2}k_{s_i} \cdot (x_{s_i}^2 + y_{s_i}^2) - \frac{1}{2}k_{c_i} \cdot (x_{c_i}^2 + y_{c_i}^2) - \frac{1}{2}k_{r_i} \cdot (x_{r_i}^2 + y_{r_i}^2) \\
- \frac{1}{2}k_{s_i t} \cdot (\theta_{s_i} r_{bs_i})^2 - \frac{1}{2}k_{c_i t} \cdot (\theta_{c_i} r_{bc_i})^2 - \frac{1}{2}k_{r_i t} \cdot (\theta_{r_i} r_{br_i})^2 - \frac{1}{2}\sum_{n=1}^{N} k_{p_i t} \cdot (\theta_{p_{i,n}} r_{bp_i})^2 \\
L_2 = \sum_{i=1}^{2}[\frac{1}{2}m_{s_i}(\dot{X}_{g_1}^2 + \dot{Y}_{g_2 x}^2) + \frac{1}{2}I_{g_i}\dot{\theta}_{g_i}^2 - \frac{1}{2}k_{g_i} \cdot (\dot{x}_{g_i}^2 + y_{g_i}^2) - \frac{1}{2}k_{g_i t} \cdot (\theta_{g_i} r_{bg_i})^2] - \frac{1}{2}k_{g_1 g_2}\delta_{g_1 g_1}^2 \\
L_3 = -\frac{1}{2}k_{s_1 c_2}(\theta_{c_2} r_{c_2} - \theta_{s_1} r_{s_1})^2 - \frac{1}{2}k_{s_2 g_1}(\theta_{g_1} r_{g_1} - \theta_{s_2} r_{s_2})^2 \\
L = L_1 + L_2 + L_3
\end{cases} \tag{12}
$$

According to lagrange equation and substituting absolute acceleration,

$$
\frac{d}{dt}\frac{\partial L}{\partial \dot{q}} - \frac{\partial L}{\partial q} = Q \tag{13}
$$

where Q is generalized force of the system.

Taking into account the meshing damping, gear backlash, TVMS and TVMF, the translation-torsion coupling dynamic equation of 42-DOF wind turbine's compound gear transmission system is obtained follows. The translation-torsion dynamic equations of the low speed stage's sun gear can be expressed as,

$$
\begin{cases}
m_{s_1}(\ddot{x}_{s_1} - 2\frac{\omega_c}{\omega_d}\dot{y}_{s_1} - \frac{\omega_c^2}{\omega_d^2}x_{s_1}) - \frac{1}{\omega_d^2}\sum_{n=1}^{N} k_{s_1 p_n} f(\delta_{s_1 p_n}) \sin(\varphi_{s_1 p_n}) - \frac{1}{\omega_d}\sum_{n=1}^{N} c_{s_1 p_n}\dot{\delta}_{s_1 p_n} \sin(\varphi_{s_1 p_n}) \\
- \frac{1}{\omega_d^2} \cdot \sum_{n=1}^{N} \lambda_{s_1 n} \cdot \mu_{s_1 n} \cdot F_{s_1 n} \cdot \cos(\varphi_{s_1 p_n}) + \frac{1}{\omega_d^2} \cdot k_{s_1} \cdot x_{s_1} = 0 \\
m_{s_1}(\ddot{y}_{s_1} + 2\frac{\omega_c}{\omega_d}\dot{x}_{s_1} - \frac{\omega_c^2}{\omega_d^2}y_{s_1}) + \frac{1}{\omega_d^2}\sum_{n=1}^{N} k_{s_1 p_n} f(\delta_{s_1 p_n}) \cos(\varphi_{s_1 p_n}) + \frac{1}{\omega_d}\sum_{n=1}^{N} c_{s_1 p_n}\dot{\delta}_{s_1 p_n} \cos(\varphi_{s_1 p_n}) \\
- \frac{1}{\omega_d^2} \cdot \sum_{n=1}^{N} \lambda_{s_1 n}\mu_{s_1 n}F_{s_1 n} \sin(\varphi_{s_1 p_n}) + \frac{1}{\omega_d^2}k_{s_1} y_{s_1} = 0 \\
M_{s_1}\ddot{u}_{s_1} + \frac{1}{\omega_d^2}\sum_{n=1}^{N} k_{s_1 p_n}\delta_{s_1 p_n} + \frac{1}{\omega_d}\sum_{n=1}^{N} c_{s_1 p_n}\dot{\delta}_{s_1 p_n} + \frac{1}{\omega_d^2}k_{s_1 t}u_{s_1} - \frac{1}{\omega_d^2} \cdot \sum_{n=1}^{N} \lambda_{s_1 n}\mu_{s_1 n}F_{s_1 n}\frac{X_{sp_{n,i}}}{r_s} \\
- \frac{1}{\omega_d^2}k_{s_1 c_2}(u_{c_2} - u_{s_1}) = 0
\end{cases} \tag{14}
$$

The translation-torsion dynamic equations of the low speed stage's planet carrier expressed as,

$$\begin{cases} m_{c_1}(\ddot{x}_{c_1} - 2\dfrac{\omega_c}{\omega_d}\dot{y}_{c_1} - \dfrac{\omega_c^2}{\omega_d^2}x_{c_1}) - \dfrac{1}{\omega_d^2}\displaystyle\sum_{n=1}^{N} k_{c_1p_n}\delta_{p_nc_1x} - \dfrac{1}{\omega_d}\sum_{n=1}^{N} c_{c_1p_n}\dot{\delta}_{p_nc_1x} + \dfrac{1}{\omega_d^2}k_{c_1}x_{c_1} = 0 \\ m_{c_1}(\ddot{y}_{c_1} + 2\dfrac{\omega_c}{\omega_d}\dot{x}_{c_1} - \dfrac{\omega_c^2}{\omega_d^2}y_{c_1}) - \dfrac{1}{\omega_d^2}\displaystyle\sum_{n=1}^{N} k_{c_1p_n}\delta_{p_nc_1y} - \dfrac{1}{\omega_d}\sum_{n=1}^{N} c_{c_1p_n}\dot{\delta}_{p_nc_1y} + \dfrac{1}{\omega_d^2}k_{c_1}y_{c_1} = 0 \\ M_{c_1}\ddot{u}_{c_1} - \dfrac{1}{\omega_d^2}\left[\displaystyle\sum_{n=1}^{N}\left(k_{s_1p_n}f_{s_1p_n} + k_{r_1p_n}f_{r_1p_n}\right) - k_{c_1}u_{c_1}\right] - \dfrac{1}{\omega_d}\sum_{n=1}^{N}\left(c_{s_1p_n}\dot{\delta}_{s_1p_n} + c_{r_1p_n}\dot{\delta}_{r_1p_n}\right) = \dfrac{T_{c_1}}{\omega_d^2 b_c r_{bc_1}} \end{cases} \tag{15}$$

The translation-torsion dynamic equations of the low speed stage's ring gear expressed as,

$$\begin{cases} m_{r_1}(\ddot{x}_{r_1} - 2\dfrac{\omega_c}{\omega_d}\dot{y}_{r_1} - \dfrac{\omega_c^2}{\omega_d^2}x_{r_1}) - \dfrac{1}{\omega_d^2}\displaystyle\sum_{n=1}^{N} k_{r_1p_n}f(\delta_{r_1p_n})\sin(\varphi_{r_1p_n}) - \dfrac{1}{\omega_d}\sum_{n=1}^{N} c_{r_1p_n}\dot{\delta}_{r_1p_n}\sin(\varphi_{r_1p_n}) \\ -\dfrac{1}{\omega_d^2}\displaystyle\sum_{n=1}^{N}\lambda_{r_1n}\mu_{r_1n}F_{r_in}\cos(\varphi_{r_1p_n}) + \dfrac{1}{\omega_d^2}k_{r_1}x_{r_1} = 0 \\ m_{r_1}(\ddot{y}_{r_1} + 2\dfrac{\omega_c}{\omega_d}\dot{x}_{r_1} - \dfrac{\omega_c^2}{\omega_d^2}y_{r_1}) + \dfrac{1}{\omega_d^2}\displaystyle\sum_{n=1}^{N} k_{r_1p_n}f(\delta_{r_1p_n})\cos(\varphi_{r_1p_n}) + \dfrac{1}{\omega_d}\sum_{n=1}^{N} c_{r_1p_n}\dot{\delta}_{r_1p_n}\cos(\varphi_{r_1p_n}) \\ -\dfrac{1}{\omega_d^2}\displaystyle\sum_{n=1}^{N}\lambda_{r_1n}\mu_{r_1n}F_{r_1n}\sin(\varphi_{r_1p_n}) + \dfrac{1}{\omega_d^2}k_{r_1}y_{r_1} = 0 \\ M_{r_1}\ddot{u}_{r_1} + \dfrac{1}{\omega_d^2}\displaystyle\sum_{n=1}^{N} k_{r_1p_n}f_{r_1p_n} + \dfrac{1}{\omega_d}\sum_{n=1}^{N} c_{r_1p_n}\dot{\delta}_{r_1p_n} + \dfrac{1}{\omega_d^2}k_{r_1t}u_{r_1} - \dfrac{1}{\omega_d^2}\sum_{n=1}^{N}\lambda_{r_1n}\mu_{r_1n}F_{r_1n}\dfrac{X_{r_1p_n}}{r_{r_1}} = 0 \end{cases} \tag{16}$$

The translation-torsion dynamic equations of the intermediate stage's sun gear is expressed as,

$$\begin{cases} m_{s_2}(\ddot{x}_{s_2} - 2\dfrac{\omega_c}{\omega_d}\dot{y}_{s_2} - \dfrac{\omega_c^2}{\omega_d^2}x_{s_2}) - \dfrac{1}{\omega_d^2}\displaystyle\sum_{n=1}^{N} k_{s_2p_n}f(\delta_{s_2p_n})\sin(\varphi_{s_2p_n}) - \dfrac{1}{\omega_d}\sum_{n=1}^{N} c_{s_2p_n}\dot{\delta}_{s_2p_n}\sin(\varphi_{s_2p_n}) \\ -\dfrac{1}{\omega_d^2}\displaystyle\sum_{n=1}^{N}\lambda_{s_2n}\mu_{s_2n}F_{s_2n}\cos(\varphi_{s_2p_n}) + \dfrac{1}{\omega_d^2}k_{s_2}x_{s_2} = 0 \\ m_{s_2}(\ddot{y}_{s_2} + 2\dfrac{\omega_c}{\omega_d}\dot{x}_{s_2} - \dfrac{\omega_c^2}{\omega_d^2}y_{s_2}) + \dfrac{1}{\omega_d^2}\displaystyle\sum_{n=1}^{N} k_{s_2p_n}f(\delta_{s_2p_n})\cos(\varphi_{s_2p_n}) + \dfrac{1}{\omega_d}\sum_{n=1}^{N} c_{s_2p_n}\dot{\delta}_{s_2p_n}\cos(\varphi_{s_2p_n}) \\ -\dfrac{1}{\omega_d^2}\displaystyle\sum_{n=1}^{N}\lambda_{s_2n}\mu_{s_2n}F_{s_2n}\sin(\varphi_{s_2p_n}) + \dfrac{1}{\omega_d^2}k_{s_2}y_{s_2} = 0 \\ M_{s_2}\ddot{u}_{s_2} + \dfrac{1}{\omega_d^2}\displaystyle\sum_{n=1}^{N} k_{s_2p_n}\delta_{s_2p_n} + \dfrac{1}{\omega_d}\sum_{n=1}^{N} c_{s_2p_n}\dot{\delta}_{s_2p_n} + \dfrac{1}{\omega_d^2}k_{s_2t}u_{s_2} - \dfrac{1}{\omega_d^2}\sum_{n=1}^{N}\lambda_{s_2n}\mu_{s_2n}F_{s_2n}\dfrac{X_{s_2p_{n,i}}}{r_{s_2}} \\ -\dfrac{1}{\omega_d^2}k_{s_2g_2}(u_{g_2} - u_{s_2}) = 0 \end{cases} \tag{17}$$

The translation-torsion dynamic equations of the low speed stage's planet gear expressed as,

$$
\begin{cases}
m_{p_1}(\ddot{x}_{p_{1,n}} - 2\dfrac{\omega_c}{\omega_d}\dot{y}_{p_{1,n}} - \dfrac{\omega_c^2}{\omega_d^2}x_{p_{1,n}}) + \dfrac{1}{\omega_d^2}k_{s_1p_{1,n}}f(\delta_{s_1p_{1,n}})\sin(\varphi_{s_1p_{1,n}}) + \dfrac{1}{\omega_d}c_{s_1p_{1,n}}\dot{\delta}_{s_1p_{1,n}}\sin(\varphi_{s_1p_{1,n}}) \\
+ \dfrac{1}{\omega_d^2}k_{r_1p_{1,n}}f(\delta_{r_1p_{1,n}})\sin(\varphi_{r_1p_{1,n}}) + \dfrac{1}{\omega_d}c_{r_1p_{1,n}}\dot{\delta}_{r_1p_{1,n}}\sin(\varphi_{r_1p_{1,n}}) \\
+ \dfrac{1}{\omega_d^2}\sum_{j=s,r}\sum_{n=1}^{N}\lambda_{jp_{1,n}}\mu_{jp_{1,n}}F_{jp_{1,n}}\cos(\varphi_{jp_{1,n}}) + \dfrac{1}{\omega_d^2}k_{c_1p_{1,n}}\delta_{p_{1,n}c_1x} + \dfrac{1}{\omega_d^2}c_{c_1p_{1,n}}\dot{\delta}_{p_{1,n}c_1x} = 0 \\
m_{p_1}(\ddot{y}_{p_{1,n}} + 2\dfrac{\omega_c}{\omega_d}\dot{x}_{p_{1,n}} - \dfrac{\omega_c^2}{\omega_d^2}y_{p_{1,n}}) - \dfrac{1}{\omega_d^2}k_{s_1p_{1,n}}f(\delta_{s_1p_{1,n}})\cos(\varphi_{s_1p_{1,n}}) - \dfrac{1}{\omega_d}c_{s_1p_{1,n}}\dot{\delta}_{s_1p_{1,n}}\cos(\varphi_{s_1p_{1,n}}) \\
- \dfrac{1}{\omega_d^2}k_{r_1p_{1,n}}f(\delta_{r_1p_{1,n}})\cos(\varphi_{r_1p_{1,n}}) - \dfrac{1}{\omega_d}c_{r_1p_{1,n}}\dot{\delta}_{r_1p_{1,n}}\cos(\varphi_{r_1p_{1,n}}) \\
+ \dfrac{1}{\omega_d^2}\sum_{j=s,r}\sum_{n=1}^{N}\lambda_{jp_{1,n}}\mu_{jp_{1,n}}F_{jp_{1,n}}\sin(\varphi_{jp_{1,n}}) + \dfrac{1}{\omega_d^2}k_{c_1p_{1,n}}\delta_{p_{1,n}cy} + \dfrac{1}{\omega_d^2}c_{c_1p_{1,n}}\dot{\delta}_{p_{1,n}c_1y} = 0 \\
M_{p_1}\ddot{u}_{p_{1,n}} + \dfrac{1}{\omega_d^2}k_{s_1p_{1,n}}\delta_{sp_{1,n}} + \dfrac{1}{\omega_d}c_{s_1p_{1,n}}\dot{\delta}_{s_1p_{1,n}} - \dfrac{1}{\omega_d^2}k_{r_1p_{1,n}}\delta_{r_1p_{1,n}} - \dfrac{1}{\omega_d}c_{r_1p_{1,n}}\dot{\delta}_{r_1p_{1,n}} \\
+ \dfrac{1}{\omega_d^2}k_{p_{1,n}t}u_{p_{1,n}} + \dfrac{1}{\omega_d^2}\sum_{j=s,r}\sum_{n=1}^{N}\lambda_{jp_{1,n}}\mu_{jp_{1,n}}F_{jp_{1,n}}\dfrac{X_{jp_{1,n}}}{r_{p_{1,n}}} = 0
\end{cases}
\tag{18}
$$

The translation-torsion dynamic equations of the intermediate stage's planet gear is expressed as,

$$
\begin{cases}
m_{p_2}(\ddot{x}_{p_{2,n}} - 2\dfrac{\omega_c}{\omega_d}\dot{y}_{p_{2,n}} - \dfrac{\omega_c^2}{\omega_d^2}x_{p_{2,n}}) + \dfrac{1}{\omega_d^2}k_{s_2p_{2,n}}f(\delta_{s_2p_{2,n}})\sin(\varphi_{s_2p_{2,n}}) + \dfrac{1}{\omega_d}c_{s_2p_{2,n}}\dot{\delta}_{s_2p_{2,n}}\sin(\varphi_{s_2p_{2,n}}) \\
+ \dfrac{1}{\omega_d^2}k_{r_2p_{2,n}}f(\delta_{r_2p_{2,n}})\sin(\varphi_{r_2p_{2,n}}) + \dfrac{1}{\omega_d}c_{r_2p_{2,n}}\dot{\delta}_{r_2p_{2,n}}\sin(\varphi_{r_2p_{2,n}}) \\
+ \dfrac{1}{\omega_d^2}\sum_{j=s,r}\sum_{n=1}^{N}\lambda_{jp_{2,n}}\mu_{jp_{2,n}}F_{jp_{2,n}}\cos(\varphi_{jp_{2,n}}) + \dfrac{1}{\omega_d^2}k_{c_2p_{2,n}}\delta_{p_{2,n}c_2x} + \dfrac{1}{\omega_d^2}c_{c_2p_{2,n}}\dot{\delta}_{p_{2,n}c_2x} = 0 \\
m_{p_2}(\ddot{y}_{p_{2,n}} + 2\dfrac{\omega_c}{\omega_d}\dot{x}_{p_{2,n}} - \dfrac{\omega_c^2}{\omega_d^2}y_{p_{2,n}}) - \dfrac{1}{\omega_d^2}k_{s_2p_{2,n}}f(\delta_{s_2p_{2,n}})\cos(\varphi_{s_2p_{2,n}}) - \dfrac{1}{\omega_d}c_{s_2p_{2,n}}\dot{\delta}_{s_2p_{2,n}}\cos(\varphi_{s_2p_{2,n}}) \\
- \dfrac{1}{\omega_d^2}k_{r_2p_{2,n}}f(\delta_{r_2p_{2,n}})\cos(\varphi_{r_2p_{2,n}}) - \dfrac{1}{\omega_d}c_{r_2p_{2,n}}\dot{\delta}_{r_2p_{2,n}}\cos(\varphi_{r_2p_{2,n}}) \\
+ \dfrac{1}{\omega_d^2}\sum_{j=s,r}\sum_{n=1}^{N}\lambda_{jp_{2,n}}\mu_{jp_{2,n}}F_{jp_{2,n}}\sin(\varphi_{jp_{2,n}}) + \dfrac{1}{\omega_d^2}k_{c_2p_{2,n}}\delta_{p_{2,n}cy} + \dfrac{1}{\omega_d^2}c_{c_2p_{2,n}}\dot{\delta}_{p_{2,n}c_2y} = 0 \\
M_{p_2}\ddot{u}_{p_{2,n}} + \dfrac{1}{\omega_d^2}k_{s_2p_{2,n}}\delta_{s_2p_{2,n}} + \dfrac{1}{\omega_d}c_{s_2p_{2,n}}\dot{\delta}_{s_2p_{2,n}} - \dfrac{1}{\omega_d^2}k_{r_2p_{2,n}}\delta_{r_2p_{2,n}} - \dfrac{1}{\omega_d}c_{r_2p_{2,n}}\dot{\delta}_{r_2p_{2,n}} \\
+ \dfrac{1}{\omega_d^2}k_{p_{2,n}t}u_{p_{2,n}} + \dfrac{1}{\omega_d^2}\sum_{j=s,r}\sum_{n=1}^{N}\lambda_{jp_{2,n}}\mu_{jp_{2,n}}F_{jp_{2,n}}\dfrac{X_{jp_{2,n}}}{r_{p_{2,n}}} = 0
\end{cases}
\tag{19}
$$

The translation-torsion dynamic equations of the intermediate stage's carrier gear is expressed as,

$$\begin{cases} m_{c_2}(\ddot{x}_{c_2} - 2\dfrac{\omega_c}{\omega_d}\dot{y}_{c_2} - \dfrac{\omega_c^2}{\omega_d^2}x_{c_2}) - \dfrac{1}{\omega_d^2}\displaystyle\sum_{n=1}^{N} k_{c_2p_n}\delta_{p_nc_2x} - \dfrac{1}{\omega_d}\sum_{n=1}^{N} c_{c_2p_n}\dot{\delta}_{p_nc_2x} + \dfrac{1}{\omega_d^2}k_{c_2}x_{c_2} = 0 \\ m_{c_2}(\ddot{y}_{c_2} + 2\dfrac{\omega_c}{\omega_d}\dot{x}_{c_2} - \dfrac{\omega_c^2}{\omega_d^2}y_{c_2}) - \dfrac{1}{\omega_d^2}\displaystyle\sum_{n=1}^{N} k_{c_2p_n}\delta_{p_nc_2y} - \dfrac{1}{\omega_d}\sum_{n=1}^{N} c_{c_2p_n}\dot{\delta}_{p_nc_2y} + \dfrac{1}{\omega_d^2}k_{c_2}y_{c_2} = 0 \\ M_{c_2}\ddot{u}_{c_2} - \dfrac{1}{\omega_d^2}\displaystyle\sum_{n=1}^{N} k_{s_2p_n}f_{s_2p_n} - \dfrac{1}{\omega_d}\sum_{n=1}^{N} c_{s_2p_n}\dot{\delta}_{s_2p_n} - \dfrac{1}{\omega_d^2}\sum_{n=1}^{N} k_{r_2p_n}f_{r_2p_n} - \dfrac{1}{\omega_d}\sum_{n=1}^{N} c_{r_2p_n}\dot{\delta}_{r_2p_n} \\ + \dfrac{1}{\omega_d^2}k_{c_2t}u_{c_2} + \dfrac{1}{\omega_d^2}k_{s_1c_2}(u_{c_2} - u_{s_1}) = 0 \end{cases} \tag{20}$$

The translation-torsion dynamic equations of fixed-axis gear are expressed as,

$$\begin{cases} m_{g_1}(\ddot{x}_{g_1} - 2\dfrac{\omega_c}{\omega_d}\dot{y}_{g_1} - \dfrac{\omega_c^2}{\omega_d^2}x_{g_1}) - \dfrac{1}{\omega_d^2}\displaystyle\sum_{n=1}^{N} k_{g_1g_2}f(\delta_{g_1g_1})\sin(\varphi_{g_1g_2}) - \dfrac{1}{\omega_d}\sum_{n=1}^{N} c_{g_1g_2}\dot{\delta}_{g_1g_2}\sin(\varphi_{g_1g_2}) \\ - \dfrac{1}{\omega_d^2}\displaystyle\sum_{n=1}^{N} \lambda_{g_1g_2}\mu_{g_1g_2}F_{g_1g_2}\cos(\varphi_{g_1g_2}) + \dfrac{1}{\omega_d^2}k_{g_1}x_{g_1} = 0 \\ m_{g_1}(\ddot{y}_{g_1} + 2\dfrac{\omega_c}{\omega_d}\dot{x}_{g_1} - \dfrac{\omega_c^2}{\omega_d^2}y_{g_1}) + \dfrac{1}{\omega_d^2}\displaystyle\sum_{n=1}^{N} k_{g_1g_2}f(\delta_{g_1g_2})\cos(\varphi_{g_1g_2}) + \dfrac{1}{\omega_d}\sum_{n=1}^{N} c_{g_1g_2}\dot{\delta}_{g_1g_2}\cos(\varphi_{g_1g_2}) \\ - \dfrac{1}{\omega_d^2}\displaystyle\sum_{n=1}^{N} \lambda_{g_1g_2}\mu_{g_1g_2}F_{g_1g_2}\sin(\varphi_{g_1g_2}) + \dfrac{1}{\omega_d^2}k_{g_1}y_{g_1} = 0 \\ M_{g_1}\ddot{u}_{g_1} + \dfrac{1}{\omega_d^2}\displaystyle\sum_{n=1}^{N} k_{g_1g_2}\delta_{g_1g_2} + \dfrac{1}{\omega_d}\sum_{n=1}^{N} c_{g_1g_2}\dot{\delta}_{g_1g_2} + \dfrac{1}{\omega_d^2}k_{g_1t}u_{g_1} - \dfrac{1}{\omega_d^2}\sum_{n=1}^{N} \lambda_{g_1g_2}\mu_{g_1g_2}F_{g_1g_2}\dfrac{X_{g_1g_2}}{r_{g_1}} = 0 \\ m_{g_2}(\ddot{x}_{g_2} - 2\dfrac{\omega_c}{\omega_d}\dot{y}_{g_2} - \dfrac{\omega_c^2}{\omega_d^2}x_{g_2}) + \dfrac{1}{\omega_d^2}\displaystyle\sum_{n=1}^{N} k_{g_1g_2}f(\delta_{g_1g_1})\sin(\varphi_{g_1g_2}) + \dfrac{1}{\omega_d}\sum_{n=1}^{N} c_{g_1g_2}\dot{\delta}_{g_1g_2}\sin(\varphi_{g_1g_2}) \\ + \dfrac{1}{\omega_d^2}\displaystyle\sum_{n=1}^{N} \lambda_{g_1g_2}\mu_{g_1g_2}F_{g_1g_2}\cos(\varphi_{g_1g_2}) + \dfrac{1}{\omega_d^2}k_{g_2}x_{g_2} = 0 \\ m_{g_2}(\ddot{y}_{g_2} + 2\dfrac{\omega_c}{\omega_d}\dot{x}_{g_2} - \dfrac{\omega_c^2}{\omega_d^2}y_{g_2}) - \dfrac{1}{\omega_d^2}\displaystyle\sum_{n=1}^{N} k_{g_1g_2}f(\delta_{g_1g_2})\cos(\varphi_{g_1g_2}) - \dfrac{1}{\omega_d}\sum_{n=1}^{N} c_{g_1g_2}\dot{\delta}_{g_1g_2}\cos(\varphi_{g_1g_2}) \\ + \dfrac{1}{\omega_d^2}\displaystyle\sum_{n=1}^{N} \lambda_{g_1g_2}\mu_{g_1g_2}F_{g_1g_2}\sin(\varphi_{g_1g_2}) + \dfrac{1}{\omega_d^2}k_{g_2}y_{g_2} = 0 \\ M_{g_2}\ddot{u}_{g_2} + \dfrac{1}{\omega_d^2}\displaystyle\sum_{n=1}^{N} k_{g_1g_2}\delta_{g_1g_2} + \dfrac{1}{\omega_d}\sum_{n=1}^{N} c_{g_1g_2}\dot{\delta}_{g_1g_2} + \dfrac{1}{\omega_d^2}k_{g_2t}u_{g_1} + \dfrac{1}{\omega_d^2}\sum_{n=1}^{N} \lambda_{g_1g_2}\mu_{g_1g_2}F_{g_1g_2}\dfrac{X_{g_1g_2}}{r_{g_2}} \\ = \dfrac{T_{g_2}}{\omega_d^2 b_c r_{bg_2}} \end{cases} \tag{21}$$

where $M_i = I_i/r_i^2$ is the equivalent mass. And $c_{pg} = 2\xi\sqrt{k_{pg}/(1/M_p + 1/M_g)}$, where ξ is the meshing damping ratio. To unify the dimension of the system, The dimensionless time parameter ω_d and the dimensionless length parameter b_c are introduced, where $\omega_d = \sqrt{k_{sp_n}/(\frac{M_s M_p}{M_s+M_p})}$.

Thus, the dimensionless equation of motion in the general coordinates can be derived in the matrix form as,

$$\mathbf{M}\ddot{q} + \mathbf{C}\dot{q} + \mathbf{K}q = F \tag{22}$$

where q is the generalized coordinate vector, **M** is the mass matrix, **C** is the damping matrix, **K** is the stiffness matrix, F is the force vector. Here, the matrix **M**, **K** and **C** are (42*42) square matrices.

3. Calculation of TVMS and TVMF

3.1. Calculation of time-varying meshing stiffness

The meshing stiffness k is a time-varying parameter, as the number of engaged teeth varies according to the contact ratio. The meshing of gear pair is divided into internal meshing and external meshing in the model of gear system.

3.1.1. Calculation of external meshing stiffness

The time-varying meshing stiffness of standard involute spur gear transmission system is solved based on the potential energy method of analytical method in this paper. According to the principle of potential energy, when the meshing force F_N acts on the tooth, the tooth will produce Hertz contact deformation and bending, compression and shear deformation, hence the four elastic potential energies: The Hertz U_h, bending U_b, axial U_a and shear U_s compressive energies can be expressed as,

$$U_h = \frac{{F_N}^2}{2K_h};\ U_b = \frac{{F_N}^2}{2K_b};U_a = \frac{{F_N}^2}{2K_a};U_s = \frac{{F_N}^2}{2K_s} \tag{23}$$

where K_h, K_b, K_a, K_s denotes the Hertz stiffness, bending stiffness, radial compression stiffness and shear stiffness corresponding to the deformation of the tooth in the direction of the meshing line under the action of the meshing force F_N.

Based on Hertz contact theory, Hertzian contact stiffness can be written as,

$$\frac{1}{K_h} = \frac{4(1-\nu^2)}{\pi E W} \tag{24}$$

where E, ν and W are Youngs modulus, Poisson's ratio and width of tooth, respectively.

Based on the beam theory, the potential energy stored in a meshing gear tooth can be expressed as,

$$\begin{cases} U_b = \dfrac{F_N^2}{2K_b} = \displaystyle\int_0^d \frac{[F_N(\cos\alpha_1)(d-x) - F_N(\sin\alpha_1)h]^2}{2EI_x}dx \\ U_a = \dfrac{F_N^2}{2K_a} = \displaystyle\int_0^d \frac{(F_N\sin\alpha_1)^2}{2EA_x}dx \\ U_s = \dfrac{F_N^2}{2K_s} = \displaystyle\int_0^d \frac{1.2F_N\cos\alpha_1}{2GA_x}dx \end{cases} \tag{25}$$

where G is the shear modulus of the material. I_x is inertia Moment of Sectional Parts with height x from meshing force. A_x is area of section:

$$G = \frac{E}{2(1+\nu)}\ , I_x = \frac{2}{3}h_x^3 W \quad A_x = 2h_x W \tag{26}$$

where K_h, K_b , K_a and K_s can be obtained according to the above formula. These four stiffnesses together with the stiffness K_f corresponding to the deformation of the gear matrix on the meshing line constitute all components of the gear time-varying meshing stiffness.

$$\begin{cases} \dfrac{1}{K_f} = \dfrac{\delta_f}{F} \\ \delta_f = \dfrac{F\cos^2\alpha_m}{WE}\left\{L^*(\dfrac{u_f}{S_f})^2 + M^*(\dfrac{u_f}{S_f}) + P^*(1+Q^*\tan^2\alpha_m)\right\} \end{cases} \tag{27}$$

Given K_h, K_b , K_a and K_s and K_f , if $\varsigma(\varsigma = 1, 2)$ is the number of meshing tooth pair, the time-varying meshing stiffness of external meshing can be calculated as,

$$K_E = \sum_{\varsigma=1}^{2}[1/(\frac{1}{K_{h,\varsigma}} + \frac{1}{K_{b1,\varsigma}} + \frac{1}{K_{s1,\varsigma}} + \frac{1}{K_{a1,\varsigma}} + \frac{1}{K_{f1,\varsigma}} + \frac{1}{K_{b2,\varsigma}} + \frac{1}{K_{s2,\varsigma}} + \frac{1}{K_{a2,\varsigma}} + \frac{1}{K_{f2,\varsigma}})] \tag{28}$$

3.1.2. Calculation of external meshing stiffness

The calculation method of time-varying meshing stiffness of internal gear tooth is the same as that of external gear tooth. Unlike the calculation of external gear, the cantilever beam cannot be equivalent to the base circle or the tooth root circle for integration. According to the geometric relations, x can be obtained,

$$\begin{cases} x = |OX|\cos\theta_x - |OF|\cos\theta_f h_x = |OX|\sin\theta_x \\ |OX| = R_b\sqrt{1+(\alpha_x+\alpha_0)^2}\theta_x = \theta_0 + \alpha_x - \arctan(\alpha_x+\alpha_0) \\ \alpha_x = \alpha_f(\alpha_d)\ \alpha_0 = \tan\alpha_r - \alpha_r + \dfrac{\pi}{2z}\ \theta_0 = \dfrac{\pi}{z} \end{cases} \tag{29}$$

where z is the number of meshing internal gear teeth, α_r is the pressure angle of meshing internal gear.

The moment of inertia of the internal gear cross section x point and its cross section area can be calculated by reference to the external meshing gear, distribution force F of gear teeth perpendicular to the center line, parallel to the center line of gear tooth and bending moment of gear tooth can be expressed as,

$$F_b = F_m\cos\alpha,\ F_a = F_m\sin\alpha,\ M = F_b x - F_a h_f \tag{30}$$

where $\alpha = \alpha_f + \theta_0$.

Since the internal gear does not consider the deformation of the matrix, the bending stiffness, radial compression stiffness and shear stiffness of the internal gear meshing tooth can be calculated as,

$$\begin{cases} \dfrac{1}{K_b} = \displaystyle\int_0^d \frac{(x\cos\alpha - h_f\sin\alpha)^2}{EI_x}dx \\ \dfrac{1}{K_s} = \displaystyle\int_0^d \frac{1.2\cos^2\alpha}{GA_x}dx \\ \dfrac{1}{K_a} = \displaystyle\int_0^d \frac{\sin^2\alpha}{EA_x}dx \end{cases} \tag{31}$$

The time-varying meshing stiffness of external meshing can be obtained as,

$$K_I = \sum_{\varsigma=1}^{2} [1/(\frac{1}{K_{h,\varsigma}} + \frac{1}{K_{b1,\varsigma}} + \frac{1}{K_{s1,\varsigma}} + \frac{1}{K_{a1,\varsigma}} + \frac{1}{K_{f1,\varsigma}} + \frac{1}{K_{b2,\varsigma}} + \frac{1}{K_{s2,\varsigma}} + \frac{1}{K_{a2,\varsigma}})] \tag{32}$$

3.1.3. Verification for the calculation method of TVMS

To test the validity of the above method, the parameters of gear pair used are the same as that in Ref. [4]. The calculation results with two methods are displayed in Fig. 2(a). For the value of single tooth meshing stiffness and double tooth meshing value of TVMS (EM), the relative errors are less than two percent, which are similar to that in Ref. [4] for CM. Therefore, the proposed method is accurate to calculate TVMS of the gear system.

Without considering the influence of meshing phase on time-varying meshing stiffness of gear, The time-varying meshing stiffness of the wind turbines gear system in two complete cycles is obtained. As shown in Fig. 2(b).

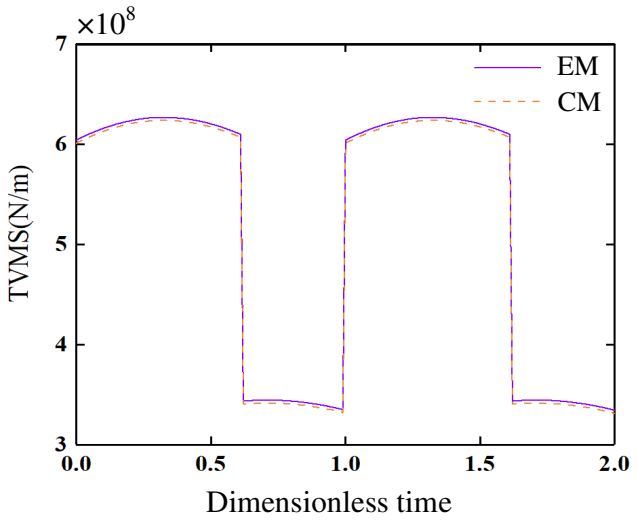

a. Calculation of TVMS with traditional method and improved method

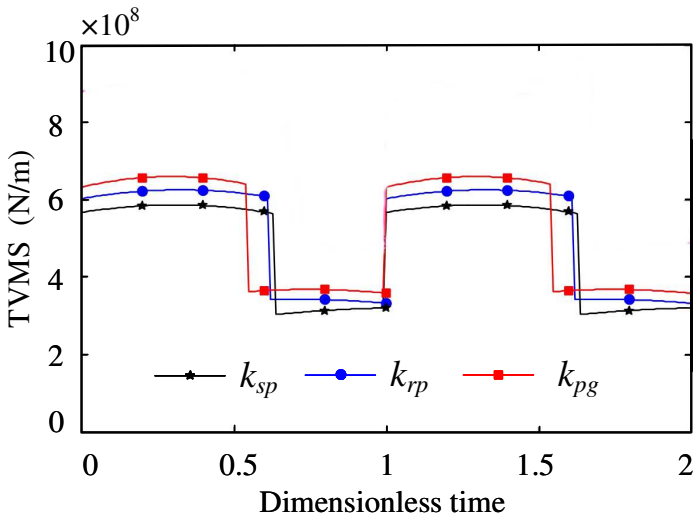

b. Calculation of the system meshing pairs' TVMS

Fig. 2. The verification and calculation of TVMS

The above time-varying meshing stiffness is expanded by Fourier series and the time-varying meshing stiffness in the form of Fourier series is obtained by deleting the high-order term,

$$k_j(t) = k_{jm} + \sum_{i=1}^{n} k_{ja} \cos(\omega t + \varphi_j) \tag{33}$$

where $k_{jm}, k_{ja}, \omega, \varphi_j$ is the equivalent average meshing stiffness, the time-varying meshing stiffness amplitude, the meshing frequency and the meshing phase angle, respectively.

3.2. An improved method for time-varying meshing friction calculation

In the process of gear transmission, the friction coefficient changes significantly with the relative sliding velocity, load distribution, temperature and tooth surface profile. In fact, the lubrication form of the wind turbine's gear meshing pairs is mixed EHL, which includes full oil film EHL and boundary lubrication. Fig.

3 depicts the moment of friction force and the internal reaction forces acting on the driving gear g and driven gear(p). The geometric relationship of meshing friction force in gear meshing process is shown in the fig. 3(a). Based on the Coulomb friction law, the magnitude of friction force (F_{fv}) is expressed as,

$$F_{fv} = \lambda \mu F_N \ (v = p, g) \tag{34}$$

where μ is the friction coefficient of mixed EHL, F_N is the dynamic meshing force of the gear pair. λ is the direction coefficient of the friction force. The normal forces acting on the driving gear,

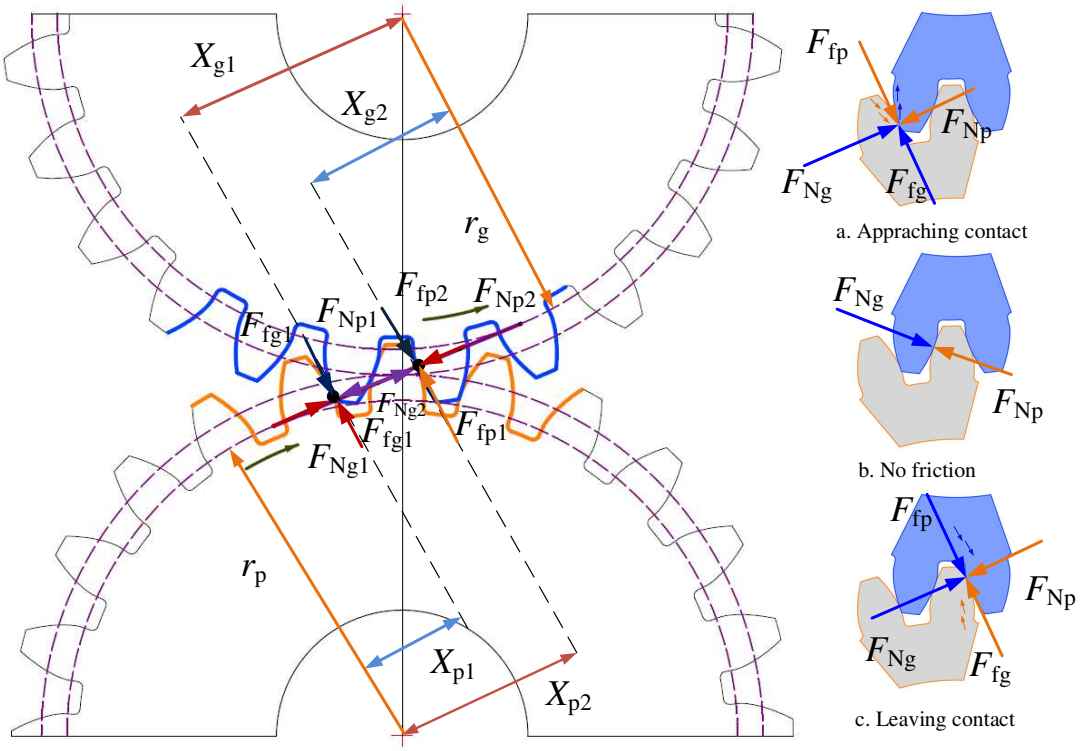

a.The meshing force arm and friction lever arm b.The meshing process

Fig. 3. The verification and calculation of TVMS

$$\begin{aligned} F_N(t) &= k_{pg}(t)[(-(x_p - x_g)\sin(\varphi_{pg}) + (y_p - y_g)\cos(\varphi_{pg}) + u_p + u_g) - E_{pg}] \\ &+ c_{pg}[(-(\dot{x}_p - \dot{x}_g)\sin(\varphi_{pg}) + (\dot{y}_p - \dot{y}_g)\cos(\varphi_{pg}) + \dot{u}_p + \dot{u}_g)] \end{aligned} \tag{35}$$

where φ_{pg} is the pressure angle. Other parameters have the same meaning as the wind turbine's gear system.

The change of friction force during meshing process can be divided into three period, which is capable to be found in Fig. 4, Fig. 4(a), Fig. 4(b) and Fig. 4(c) are approaching contact, no friction and leaving contact process, respectively. λ represents the change of force direction in meshing process,

$$\lambda(t) = \begin{cases} 1 & \omega_p X_{pi}(t) > \omega_g X_{gi}(t) \\ 0 & \omega_p X_{pi}(t) = \omega_g X_{gi}(t) \\ -1 & \omega_p X_{pi}(t) < \omega_g X_{gi}(t) \end{cases} \tag{36}$$

Where ω_v is the meshing frequency, $X_{pi}(t)$, $X_{gi}(t)$ stand for the length of the time-varying friction lever arm of the ith gear tooth of pinion and gear, respectively and are given by,

$$\begin{cases} X_{pi}(t) = (r_p + r_g)\tan\alpha - \sqrt{r_p^2 - r_g^2} + r_p\omega t \\ X_{gi}(t) = \sqrt{r_p^2 - r_g^2} - r_p\omega t \end{cases} \tag{37}$$

where r_v is base radius. α is meshing angle.

The friction coefficient of mixed EHL can be introduced as,

$$\mu = \zeta\mu_{EHL} + (1-\zeta)\mu_B \tag{38}$$

The boundary lubrication friction coefficient μ_B measured through experiments is generally 0.10.2. The full oil film EHL coefficient μ_{EHL} can be expressed as,

$$\begin{cases} \mu_{EHL} = \exp[f(SR, F_N, \eta_0, \sigma)]ph^{b_2}|SR|^{b_3}{v_r}^{b_6}{\eta_0}^{b_7}R^{b_8}\xi^{0.2} \\ f(SR, F_N, \eta_0, \sigma) = b_1 + b_4 ph\,|SR|\log_{10}^{\eta_0} + b_5\exp[-F_N\,|SR|\log_{10}^{\eta_0}] + b_9\exp[\sigma] \\ SR = 2\left|\dfrac{(z_p+z_g)(\tan(\alpha)-\tan(\alpha_{k1}))}{(z_p+z_g)\tan(\alpha)+(z_p-z_g)\tan(\alpha_{k1})}\right| \\ R = r_{pb}\tan(\alpha_{k1}) - \dfrac{r_{pb}z_p}{(z_p+z_g)\tan(\alpha)}\tan(\alpha_{k1})^2 \\ v_r = \dfrac{\left|mz_p\omega\cos(\alpha)[\tan(\alpha)(z_p+z_g)+(z_p-z_g)\tan(\alpha_{k1})]\right|}{2z_g} \\ v_s = \left|\dfrac{mz_p\omega(z_p+z_g)\cos(\alpha)}{2z_g}(\tan(\alpha)-\tan(\alpha_{k1}))\right| \end{cases} \tag{39}$$

where η_0 is the absolute viscosity at oil inlet temperature, SR is the slide-roll ratio of the gear pair, v_r and v_s is the relative sliding velocity and rolling velocity at contact point, $b_i(i = 1, 2, s, 9)$ are constant coefficients that are dependent on the lubricant type. For ISO-VG-220 gear oil, $b_1 = -8.9$, $b_2 = 1.1$, $b_3 = 1$, $b_4 = -0.3$, $b_5 = 2.8$, $b_6 = -0.1$, $b_7 = -0.7$, $b_8 = -0.4$, $b_9 = -0.6$.

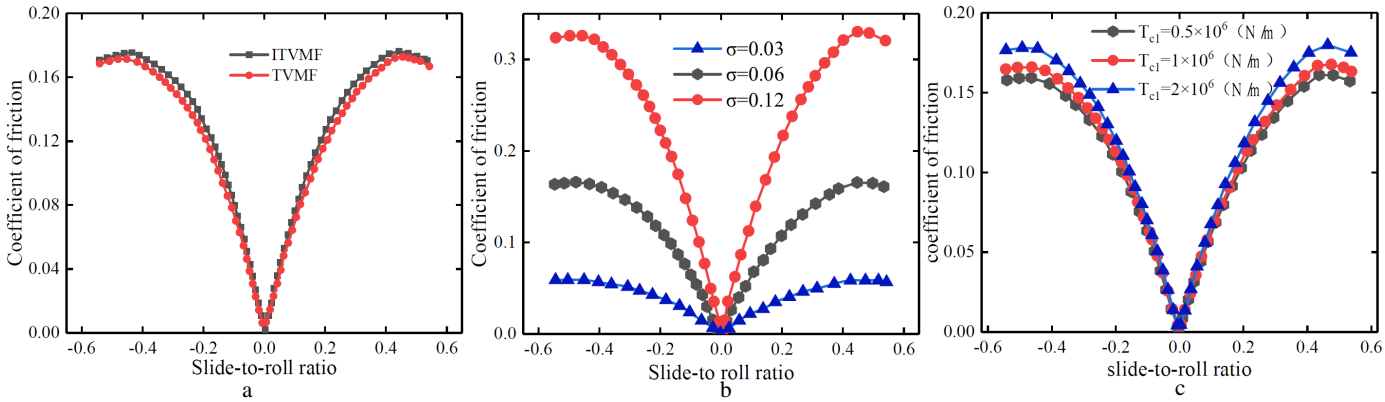

Fig. 4. The verification and calculation of TVMF

The friction coefficient of mixed EHL $\zeta(0 < \zeta < 1)$ is related to the load distribution percentage function. Based on a large number of experiments and numerical calculations, the load distribution percentage coefficient be expressed as

$$\begin{cases} \zeta = 1.21(h_{\min}/\sigma)^{0.64}/[1 + 0.37(h_{\min}/\sigma)^{1.26}] \\ h_{\min} = 1.6\alpha_p^{0.6}(\eta_0 v_m)^{0.7} R^{0.43} E^{0.43}/\bar{w}^{0.13} \end{cases} \tag{40}$$

where h_{min} is the minimum oil film thickness, σ is the root mean square(RMS) of roughness, α_p is the viscosity coefficient, v_m is the average speed of tooth surface meshing, $\bar{w}$ is the load coefficient.

3.2.1. Verification for the calculation method of TVMF

To test the validity of the above method, the parameters of gear pairs used are the same as those in Ref. [17]. Comparison of calculation results of two Methods from Fig. 4(a), the calculation results ITVMF of the above method are consistent with those in Ref. [17] for TVMF. Therefore, the proposed method can accurately calculate the friction coefficient of wind turbine's spur gears. In order to further study the influence of other parameters on the friction coefficient, Fig. 4(b,c) give the effect of surface roughness and input torque. As Fig. 4(b) shows, as absolute values of slide-to-roll ratio and surface roughness increasing, the coefficient of friction increases, surface roughness has great influence on friction coefficient. As could be deduced from Eq. (39), the coefficient is directly related to meshing force F_N, whice is determined by input torque(T_{c_1}). Fig. 4(c) indicates the TVMF under different (T_{c_1}). Thus, with the increase of T_{c_1}, the friction coefficient increases.

4. Nonlinear dynamic response of the CGTS

The parameters of the CGTS are listed in Table 1. Other calculation parameters are shown in table 2. The coupled dynamic equations are solved by the Runge-Kutta method. For better analysis the dynamic characteristics of the CGTS, more numerical computations are carried out and the dynamic responses of gear system are obtained. In order to study the effect of friction on the dynamic response of the system, the timedomain curves of dimensionless relative vibration displacement of internal and external meshing gear pairs are obtained without and with the effect of friction, as shown in Fig. 5.

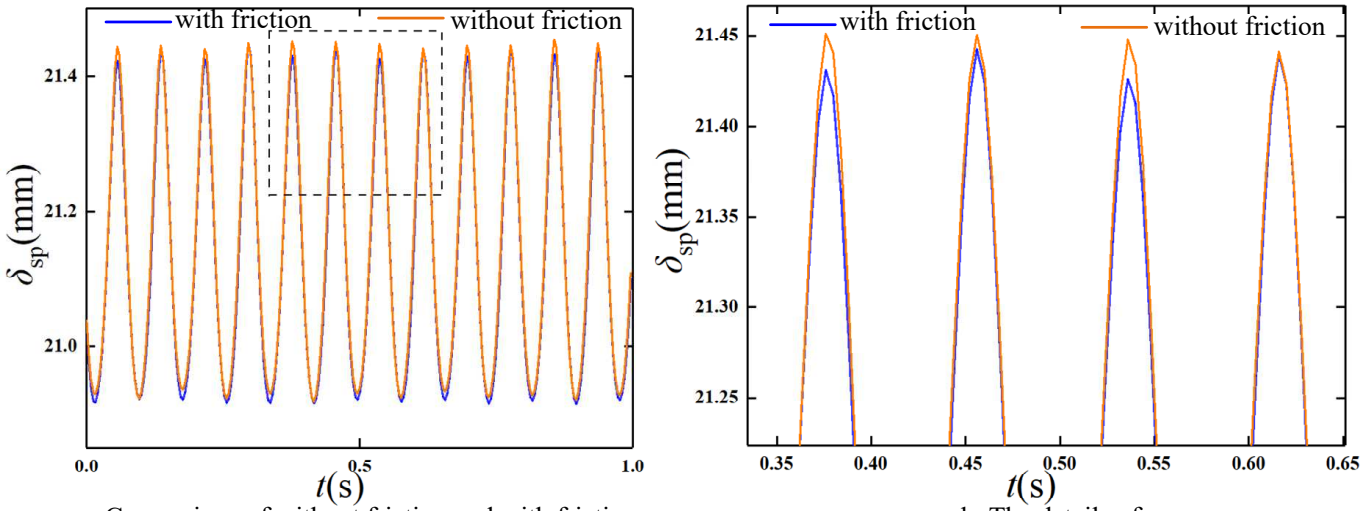

a. Comparison of without friction and with friction

b. The details of a

Fig. 5. Timedomain comparison curve of dimensionless relative vibration displacement δ_{sp}

Table 1. This is a test basic parameters of gear system.

Parameters	carrier (c_1/c_2)	Sun (s_1/s_2)	Planet (p_1/p_2)	Ring (r_1/r_2)	Gear(g_1)	Pinion(g_2)
Number of teeth, Z	-	31/22	47/41	125/104	73	25
Mass, M/kg	2042/1212	345/131	388/176	410/80	208	24
Moment of inertia, I/(kg mm^2)	463/152	8/1.5	16/5	226/26	8.87	0.12
Module, m/mm	-	14/10	14/10	14/10	4	
Average stiffness, N/m	-	1.31×10^{10}		1.48×10^{10}	2.453×10^{10}	
Amplitude stiffness, N/m	-	4.96×10^{9}		5.12×10^{9}	5.31×10^{9}	
Modulus of elasticity, E/Gpa	206					
Poissons ratio, P	0.3					
RMS value of roughness, σ/um	0.06					
Ambient viscosity of lubricant, η_0/pa$s$	0.01					
Viscosity pressure coefficient of lubricant, α_p/pa^{-1}	2.19×10^{-8}					
Load coefficient, ϖ	0.3					
Addendum coefficient, h_a	1					
Number of planets, N	3					
pressure angle, α	22.5					
Meshing damping ratio, ξ	0.07					

Table 2. This is operation parameters of gear system.

Parameters	Low speed stage	Intermediate stage	High speed stage
Transmission ratio	5.25	5.28	2.92
Rated input torque,T_c(N/m)	1×10^{6}		
Rated input torque,T_{g_2}(N/m)			1.23×10^{4}
Rated input speed, n/min	18		
Coupling stiffness, N/m	$k_{s_1c_2}$=5×10^{9}	$k_{s_2g_1}$=5×10^{9}	
Dimensionless nominal length, $b_c(\mu m)$	10		
Dimensionless gear backlash	2		
Dimensionless error amplitude	2		

It can be seen from Fig. 5 that when the effect of friction is considered, the dimensionless relative vibration displacement amplitude decrease. The friction force increase the peak difference of the dimensionless relative vibration displacement amplitude and makes the periodicity of the system complex, which is consistent with the conclusion in the literatures[3]. The correctness of the model and simulation results can be verified. Because the vibration characteristics of the internal and external meshing pairs are consistent, the relative displacement of the external meshing pair δ_{sp} is analyzed for the dynamic characteristics as an example.

4.1. Effect of excitation frequency

The speed of the wind turbine's gear transmission system is the most important external excitation of the gear system, which corresponds to the excitation frequency (Ω) in the gear system. When the dimensionless excitation frequency Ω is considered as the bifurcation parameter, the bifurcation diagram of the wind turbine's gear tranmission system is shown in Fig. 6. It can be seen from the Fig. 6 that the wind turbine's gear transmission system has rich bifurcation and chaos behaviors, in which includes single-period, multi-period, quasi-period and chaotic motion. The system first undergoes periodic motion in the low frequency region, then enters chaotic motion. In chaotic region, system appears two periodic windows. Finally, system changes from chaotic motion to single-period motion through inverse doubling bifurcation. To display the dynamic characteristics more clearly, time region diagrams, poincare maps, phase diagrams and amplitude-frequency spectrums are obtained to analyze the nonlinear characteristics of the wind turbine's gear tranmission system in detail.

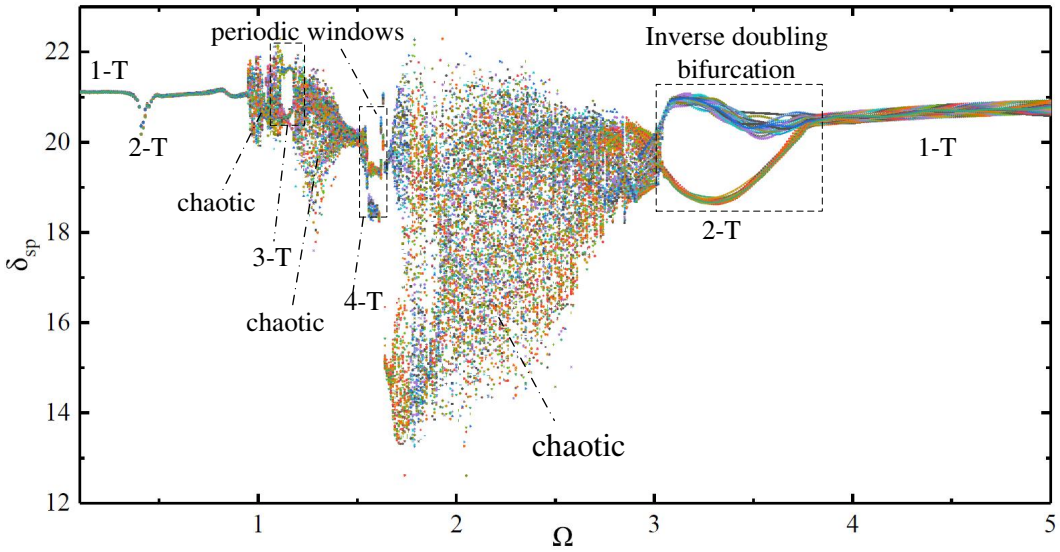

Fig. 6. Bifurcation diagram using frequency ratio as control parameter

When Ω is less than 0.4, It can be seen from Fig. 6 that the bifurcation diagram presents a single point. Time region diagram exhibits regular single-amplitude sine wave, and phase diagram shows one close loop. Poincare map has only one point, and amplitude-frequency spectrum has one-peak amplitude, as shown in Fig. 7. Obviously the gear system is periodic-1 motion under low frequency excitation. Corresponding to the wind turbine at low rotational speed, the operation of the gear system is relatively stable.

When Ω is increased to 0.42, It can be seen from Fig. 8 that time domain diagram appear two peaks in one period, there are two closed circles in phase diagram, and Poincare map shows two points. Moreover, the amplitude-frequency spectrum has two peaks amplitude, the system state is changed from periodic-1 to periodic-2 motion. Corresponding to the wind turbine's gear system, there is a multi-period window in the single-periodic region.

When Ω is changed from 0.43 to 0.97, the systems motion is periodic-1 motion. With Ω increases to 0.98, the system turns to chaotic motion. As shown in Fig. 9, time domain diagram appears irregular vibration and phase diagram show irregular countless closed motion, and the chaotic motion can be verified by irrgular discrete points in projection of Poincare map and amplitude-frequency spectrum display multiple amplitudes.

When Ω increases to 1.12, the system appear periodic window in chaotic region. For example, when Ω=1.15, the time domain diagram has three amplitude changes in a period. there are three discrete points on the

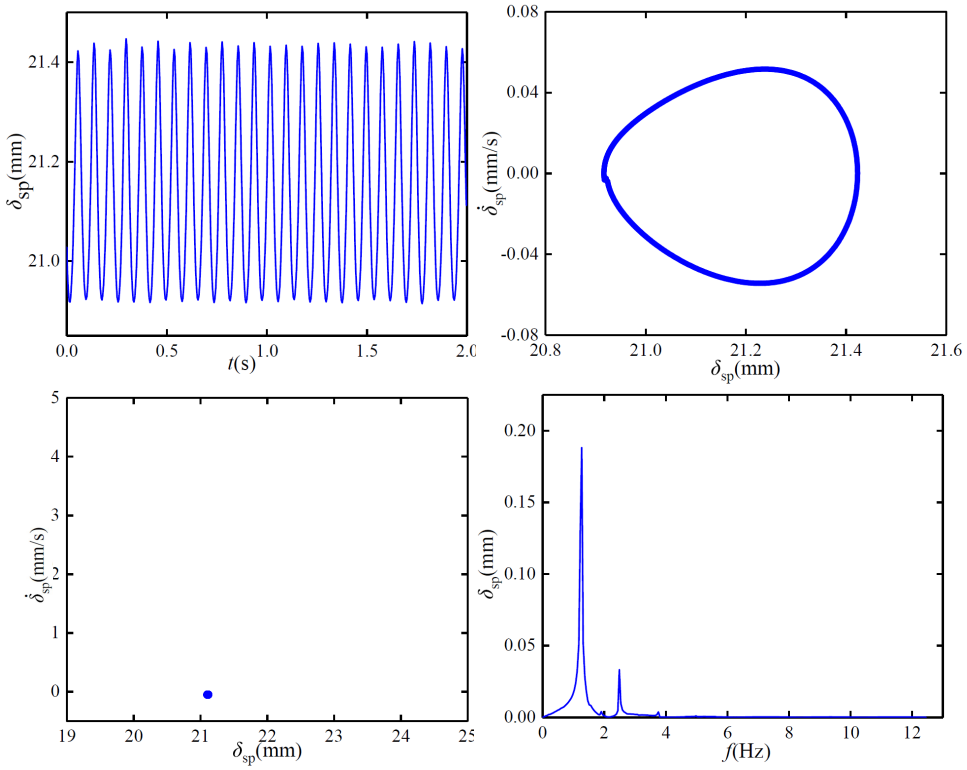

Fig. 7. The dynamic characteristic curve of the system at Ω = 0.4.

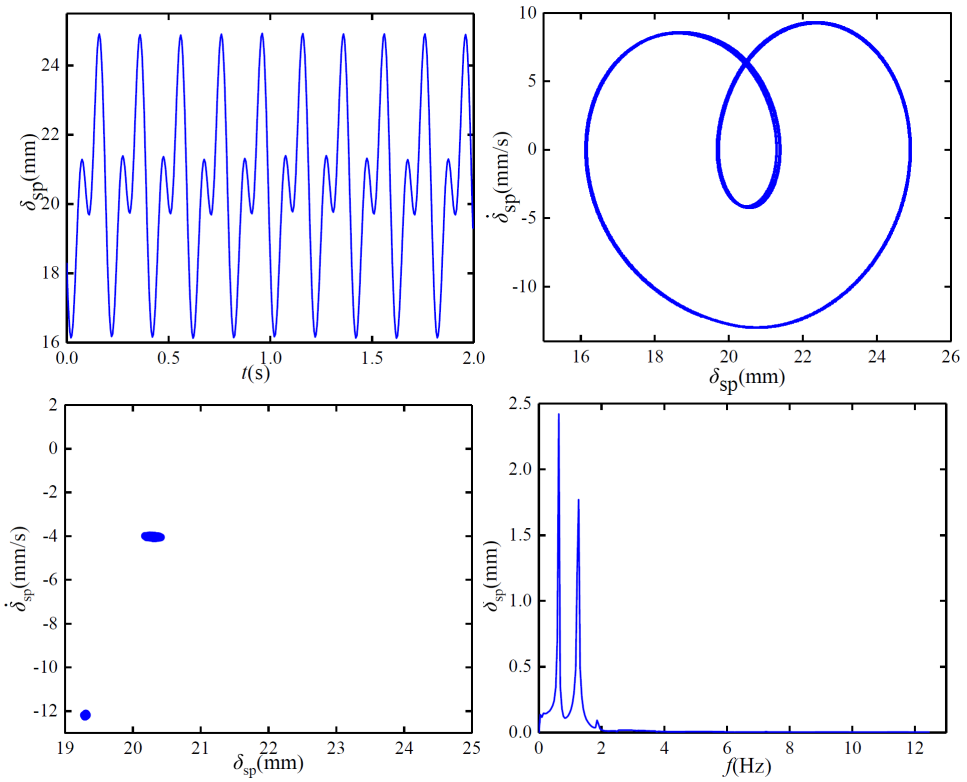

Fig. 8. The dynamic characteristic curve of the system at Ω = 0.42.

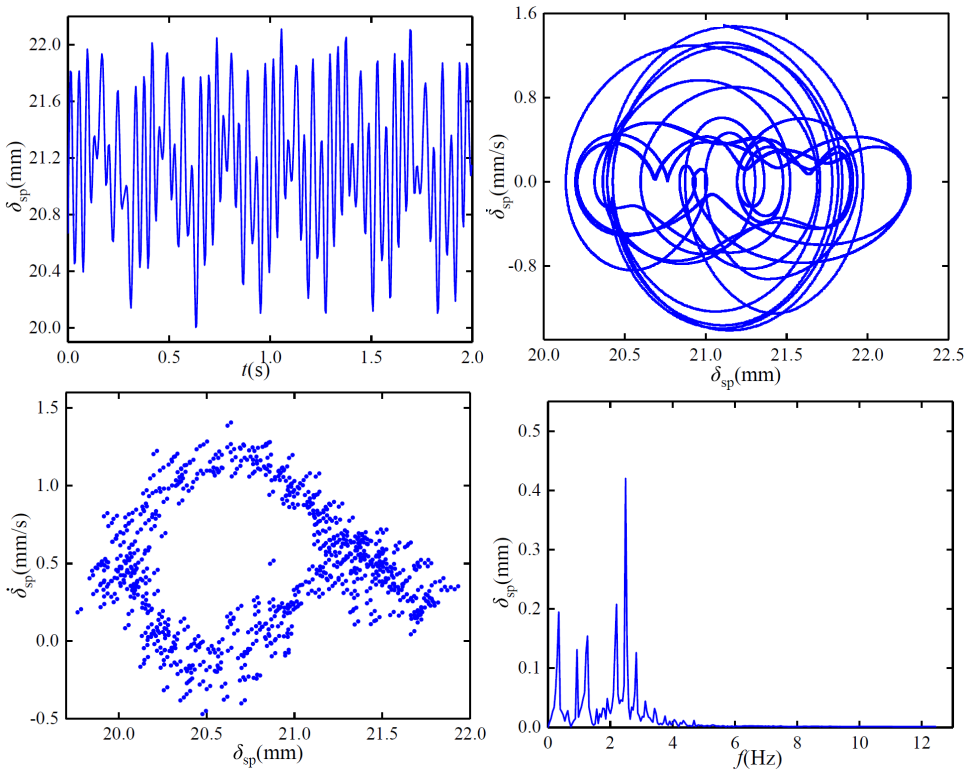

Fig. 9. The dynamic characteristic curve of the system at Ω = 0.98.

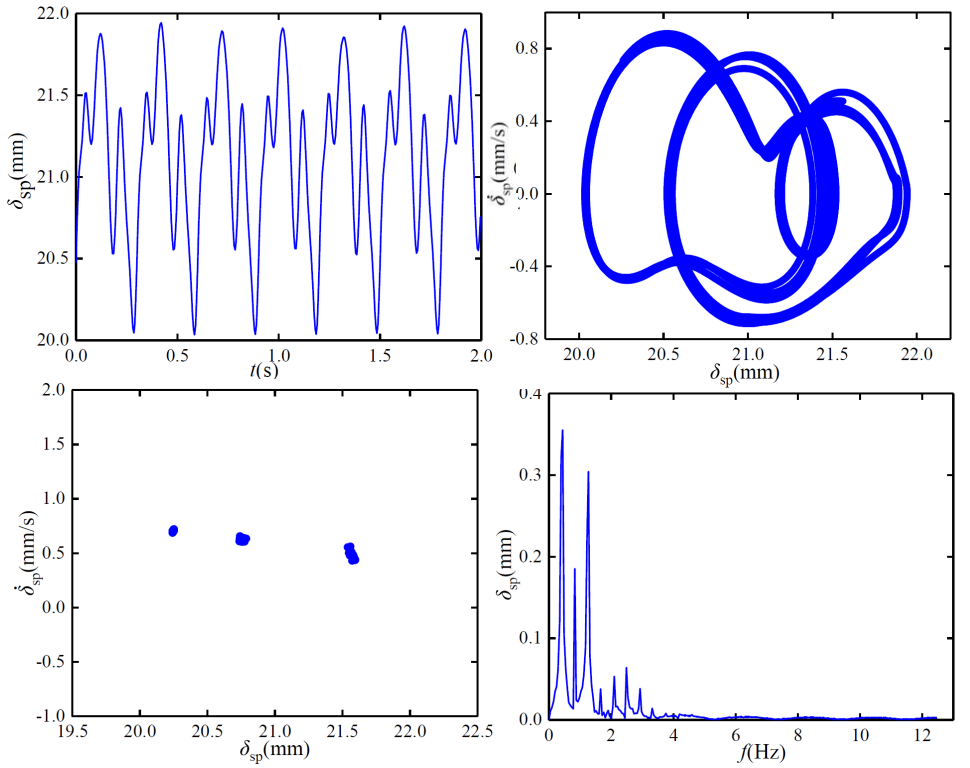

Fig. 10. The dynamic characteristic curve of the system at Ω = 1.15.

Poincare map. The phase diagram is a closed pattern formed by three periods of phase trajectories. Poincare map is three fixed points. There are three peaks in the amplitude spectrum, which appear at one third and two thirds of the fundamental frequency, respectively. Obviously the system is periodic-3 motion. As shown in Fig. 10.

When Ω increases to 1.18, it is can be seen from Fig. 6 that the system turns to chaotic motion. When Ω continues to increase to 1.52, the systems appear periodic window again, including periodic-4 motion; when Ω reaches to 1.66, the time domain diagram, phase diagram, Poincare map and amplitude-frequency spectrum corresponding to the chaotic response are presented in Fig. 11. Obviously, the system is in chaotic state under this excitation frequency. In the working process of the wind turbine, the operation under the excitation frequency of this region should be avoided as far as possible.

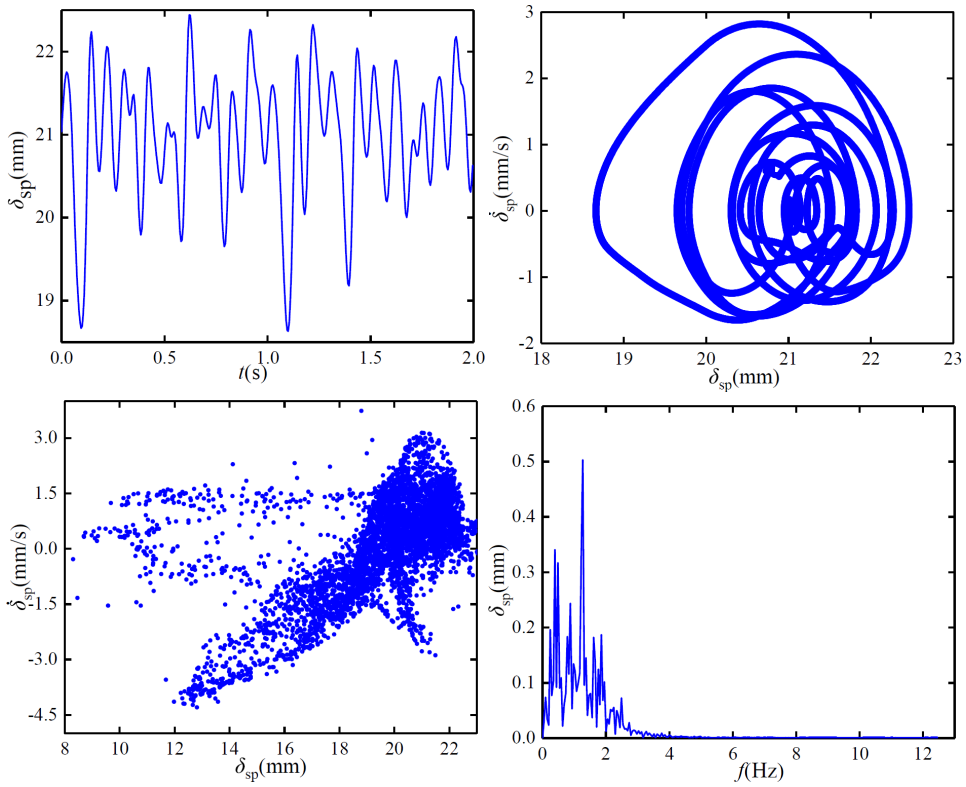

Fig. 11. The dynamic characteristic curve of the system at Ω = 2.

With the increasing of Ω, the system turns to periodic-2 motion which remains the state from 3.05 to 3.76. When Ω is equal to 3.15, time domain diagram appear two peaks in one period, there are two closed circles in phase diagram, and Poincare map shows two points. The amplitude-frequency spectrum has two peaks amplitude, which are distributed at discrete points of Ω/2. as illustrated in Fig. 12.

When Ω continues to increases to 3.77, the system finally returns to periodic-1 motion. the time domain diagram, phase diagram, Poincare map and amplitude-frequency spectrum corresponding to periodic-1 response are presented in Fig. 13. In engineering practice, the excitation frequency corresponds to the speed of the wind turbines gear transmission system. In order to make the wind turbine's transmission gear system have better stability and reliability and prolong the working cycle life, wind turbine should avoid the speed range of chaotic motion and the critical speed of changing state.

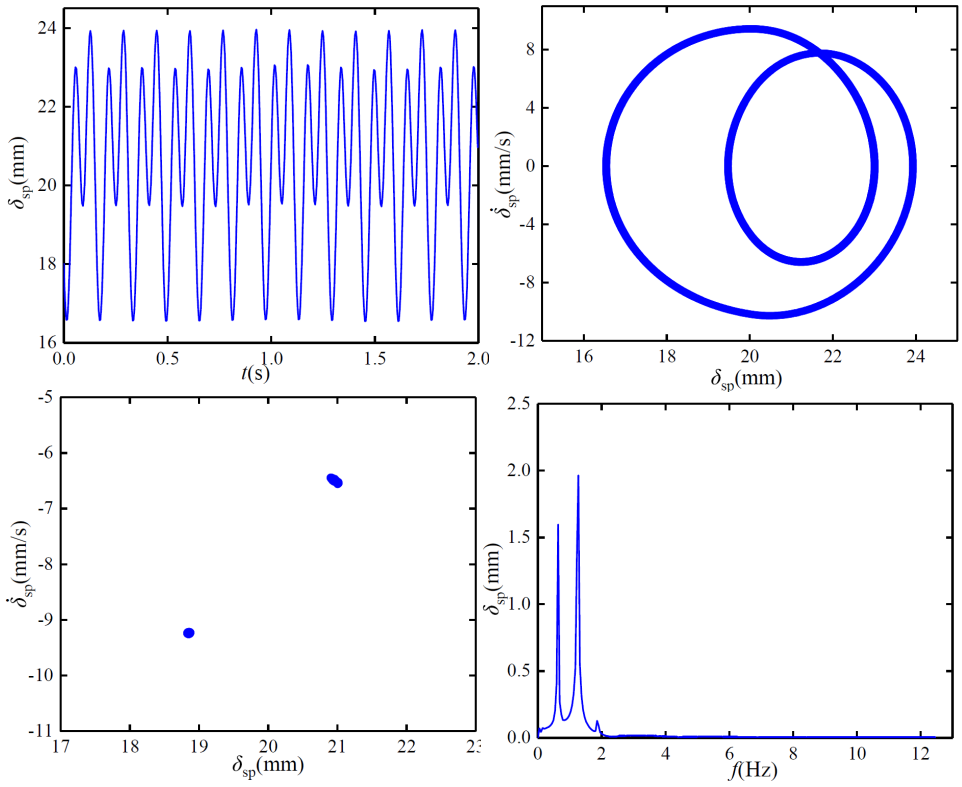

Fig. 12. The dynamic characteristic curve of the system at Ω = 3.15.

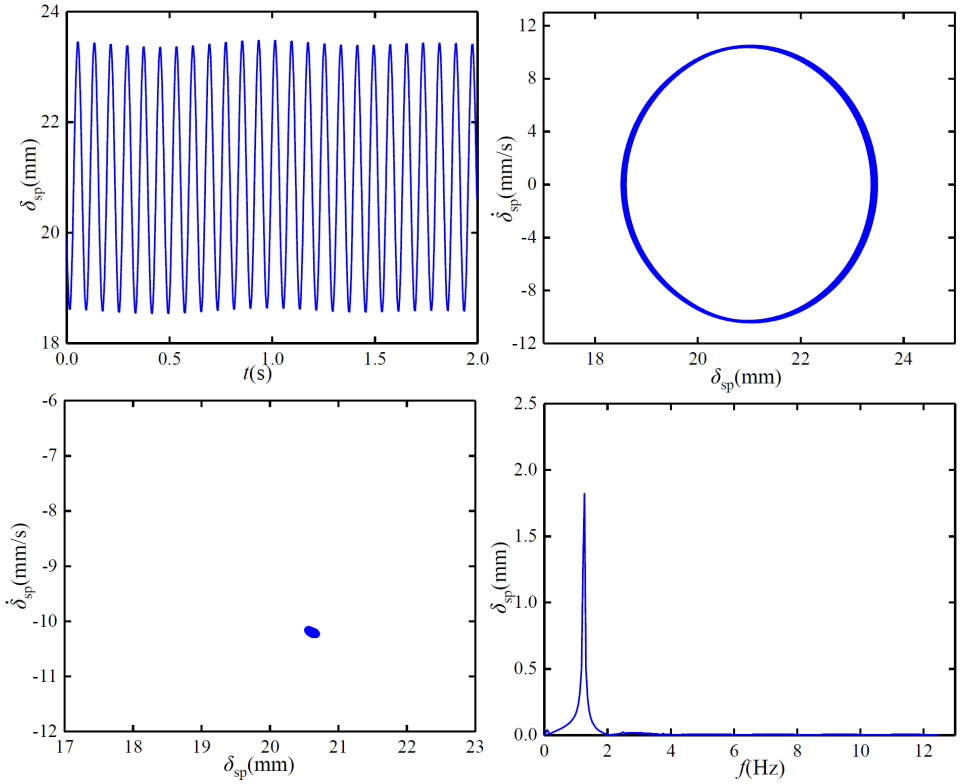

Fig. 13. The dynamic characteristic curve of the system at Ω = 4.2.

4.2. Effect of friction on Bifurcation Characteristics

The bifurcation characteristics is also one of the main nonlinear dynamic of gear system. Thus, it is necessary to study the influence of friction on the Bifurcation characteristics of gear system. Fig. 14 shows the bifurcation diagram of the dimensionless displacement δ_{sp} using the excitation frequency Ω as bifurcation parameter when using different RMS of roughness (σ=0.03,0.06), and the other parameters remain the same as the previous section.

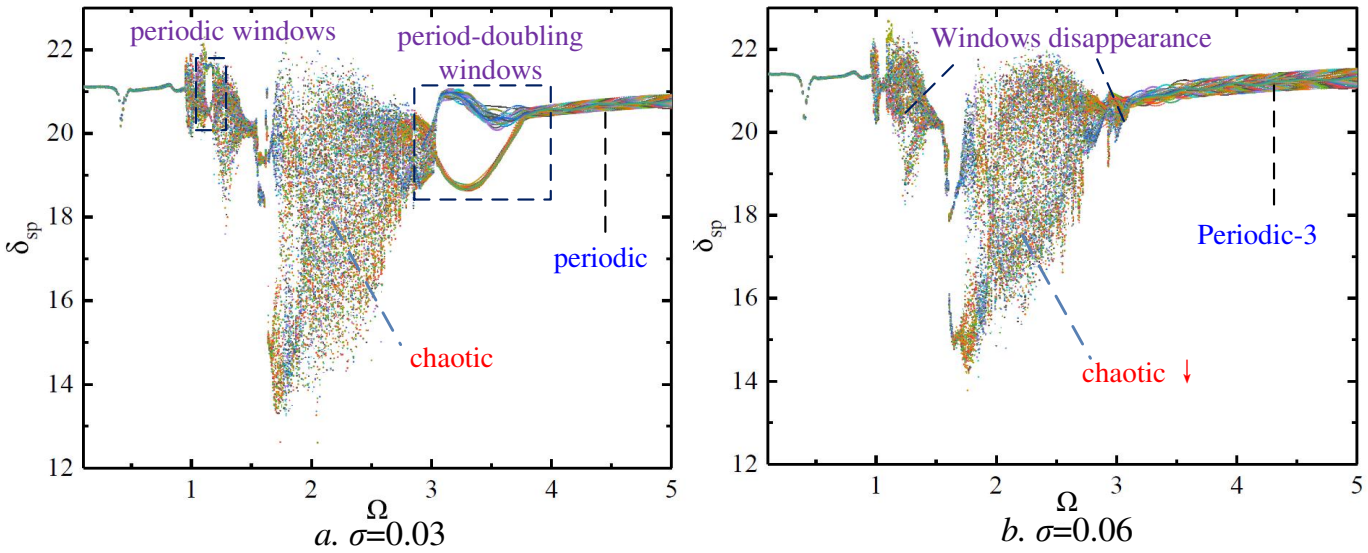

Fig. 14. Bifurcation diagram of the system with Ω

It can be seen from Fig. 14(a, b) that the bifurcation behavior of the system is basically unchanged with the increase of RMS of roughness in the low frequency region, indicating that friction has little effect on the low frequency region.

When is equal to 1.15, phase diagrams infinitely loop in the enclosed area, but never duplicates. The return points in Poincare maps form a geometrically fractal structure, and amplitude-frequency spectrum is continuous. the systems motion is in state of chaos, as shown in Fig.15. Thus, When is changed from 1.12 to 1.18, the periodic window of the chaotic region disappears. When is equal to 2, the fluctuation of time domain curve tends to be smooth, Discrete points of Poincare maps is more concentrated. as shown in Fig. 16.

Through comparing Fig. 11 and Fig. 17, the peak number of amplitude-frequency spectrum decreases. The chaotic characteristics of system attenuate. It can be seen from Fig. 14(a,b) that with the increase of RMS of roughness, the periodic window of inclusions in the chaotic region of the system disappears in the high frequency region.

When is equal to 3.15, as shown in Fig. 17. The quasi-periodic motion of the system changes into chaotic motion, resulting in an increase in the chaotic region. The motion state of the system changes, the bifurcation behavior becomes complicated.

When is more than 3.27, the system enters periodic-3 motion, as shown in Fig. 18, which indicates that friction has a great influence on the high frequency region. From the above analysis, the multiple periodic motion of the system decreases, the chaotic motion region increases, and the critical frequency of entering the chaotic motion is advanced in the high frequency region when RMS of roughness increase.

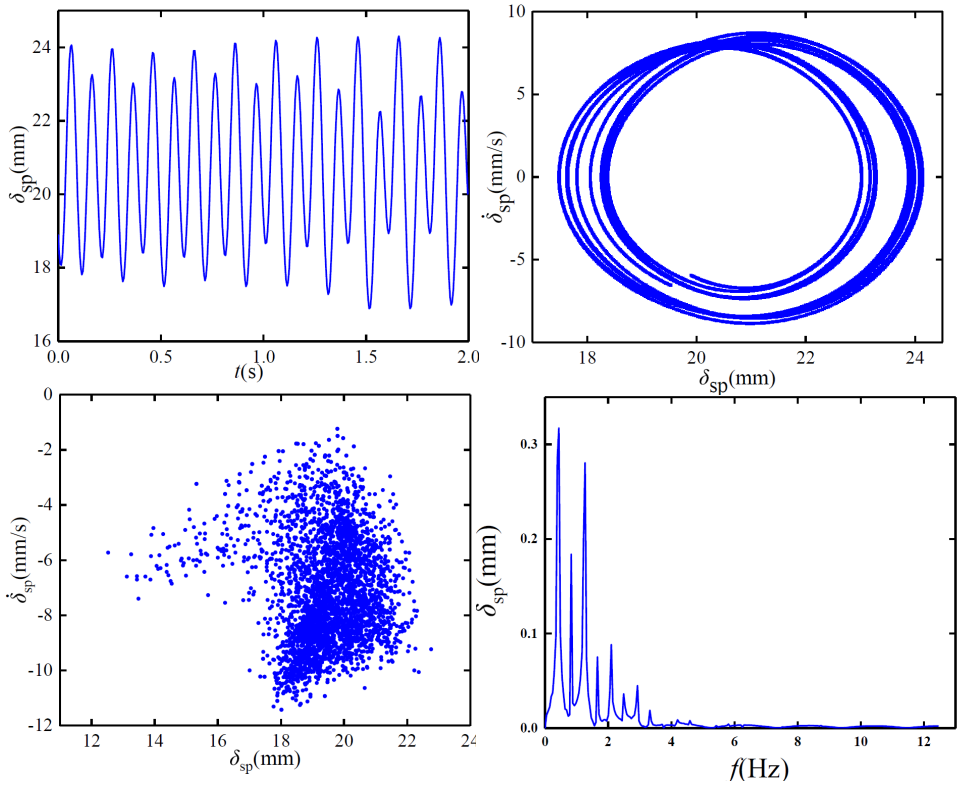

Fig. 15. The dynamic characteristic curve of the system at Ω = 1.15.

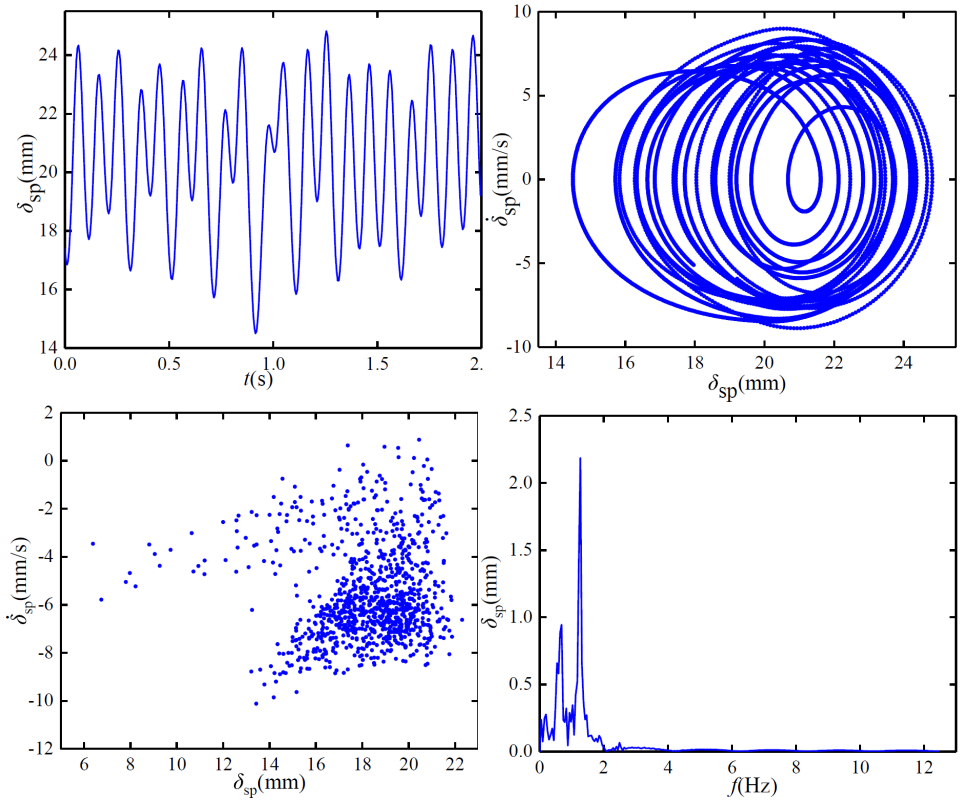

Fig. 16. The dynamic characteristic curve of the system at Ω = 2.

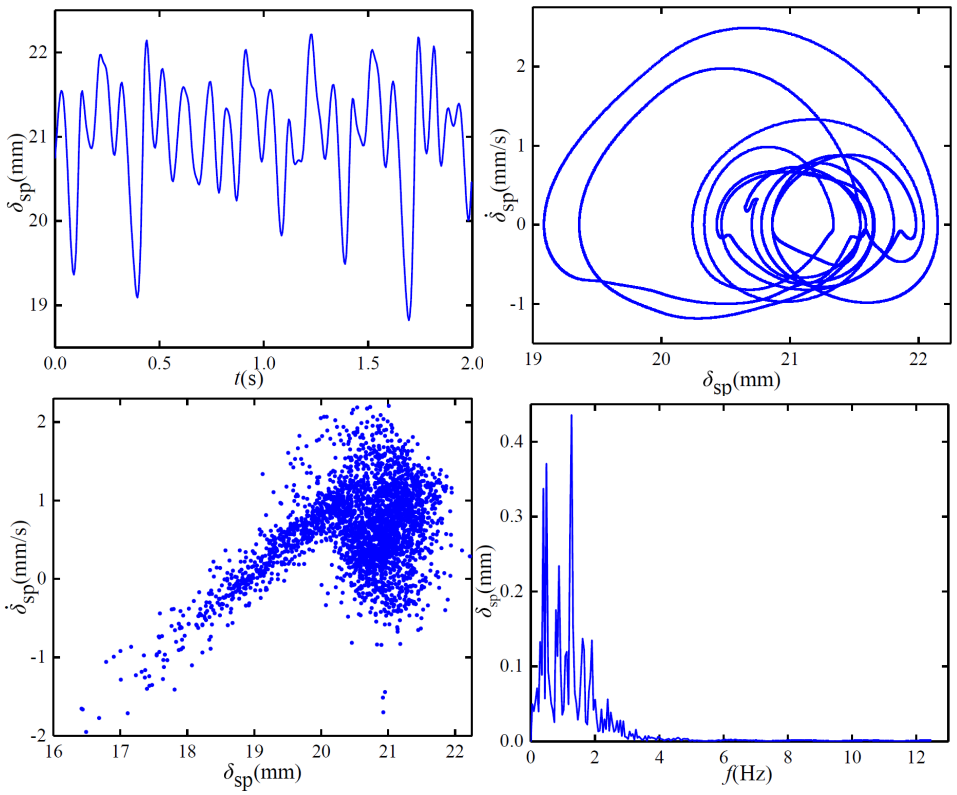

Fig. 17. The dynamic characteristic curve of the system at Ω = 3.15.

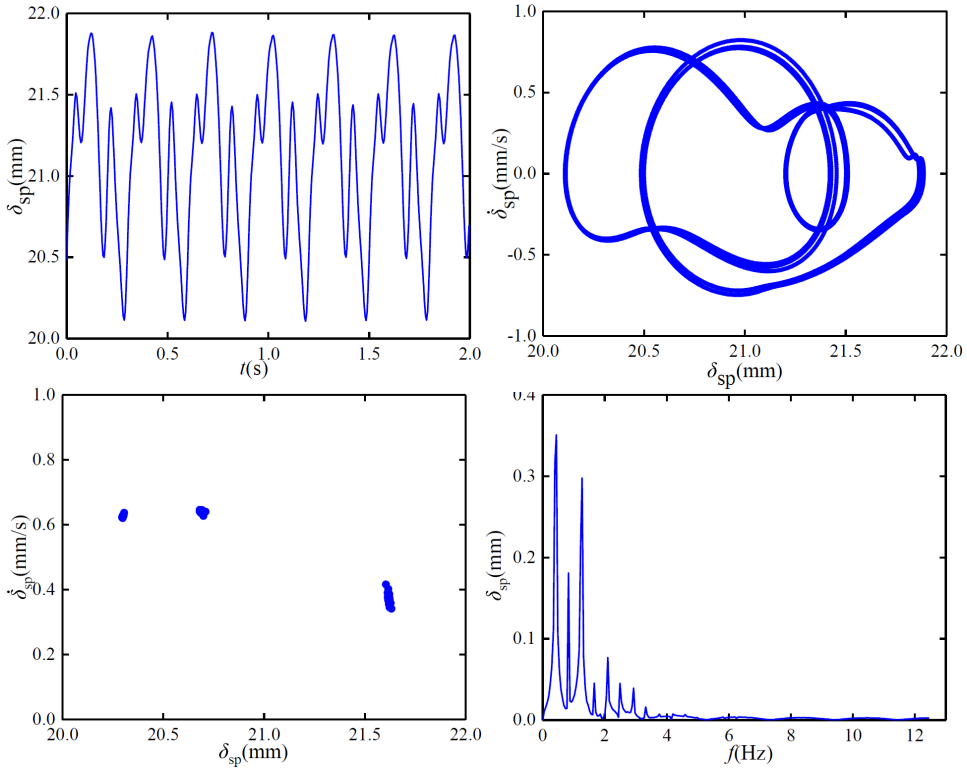

Fig. 18. The dynamic characteristic curve of the system at Ω = 4.2.

5. Conclusion

A 42-DOF translation-torsion coupling dynamics model of the wind turbines gear transmission system considering TVMS, TVMF, meshing damping, meshing error and backlash is established. The dynamic characteristics of the wind turbines gear transmission system are studied, which is solved by the RungeKutta numerical method, and the conclusions are as follow:

- Considering the TVMS and TVMF, the system frequency is an important parameter. For some values of the frequency ratio (i.e,2<Ω<3.15), the system gets into multi-period and chaos motion state. In these cases, the vibration state of the system is disordered, and such vibration frequency should be avoided as far as possible.
- Mix-EHL is more in line with the engineering practice,which includes boundary friction and EHL. When friction is considered, the friction has little effect on the bifurcation behavior of the system in the low frequency region. In the high frequency region, the bifurcation behavior of the system becomes complicated and the chaotic region increases.
- With the increase of friction coefficient, the periodic window of the system disappears in the low frequency region, the multiple periodic motion regions decrease in the high frequency region, and the chaotic motion interval of the system increases.

Acknowledgements

The research reported in the paper is part of the projects supported by National Natural Science Foundation of China (Grant no.52075392).

Conflict of Interest

The authors declare that they have no conflict of interest.

Data Availability Statements

The datasets generated during and analysed during the current study are available from the corresponding author on reasonable request.

References

[1] WU Shijing, Ren Hui,et al. Research advances for dynamics of planetary gear trains[J]. Engineering Journal of Wuhan University, 2010, 43(3):398-403.

[2] J. LIN, R.G. PARKER, Sensitivity of planetary gear natural frequencies and vibration modes to model parameters, J SOUND VIB, 228 (1999) 109-128.

[3] V.K. Ambarisha, R.G. Parker, Nonlinear dynamics of planetary gears using analytical and finite element models, J SOUND VIB, 302 (2007) 577-595.

[4] S. Zhou, Z. Ren, G. Song, B. Wen, Dynamic Characteristics Analysis of the Coupled Lateral-Torsional Vibration with Spur Gear System, International Journal of Rotating Machinery, 2015 (2015) 1-14.

[5] J. Wang, N. Liu, H. Wang, L. Guo, Nonlinear dynamic characteristics of planetary gear transmission system considering squeeze oil film, Journal of Low Frequency Noise, Vibration and Active Control, (2020) 146134842093566.

[6] J. Wang, J. Zhang, Z. Yao, X. Yang, R. Sun, Y. Zhao, Nonlinear characteristics of a multi-degree-of-freedom spur gear system with bending-torsional coupling vibration, MECH SYST SIGNAL PR, 121 (2019) 810-827.

[7] Z. Zhu, L. Cheng, R. Xu, R. Zhu, Impacts of Backlash on Nonlinear Dynamic Characteristic of Encased Differential Planetary Gear Train, SHOCK VIB, 2019 (2019).

[8] S. He, R. Gunda, R. Singh, Effect of sliding friction on the dynamics of spur gear pair with realistic time-varying stiffness, J SOUND VIB, 301 (2007) 927-949.

[9] S. He, R. Gunda, R. Singh, Inclusion of sliding friction in contact dynamics model for helical gears, J MECH DESIGN, 129 (2007) 48-57.

[10] S. Li, A. Kahraman, A tribo-dynamic model of a spur gear pair, J SOUND VIB, 332 (2013) 4963-4978.

[11] S. LI, A. KAHRAMAN, A Method to Derive Friction and Rolling Power Loss Formulae for Mixed Elastohydrodynamic Lubrication, Journal of Advanced Mechanical Design, Systems, and Manufacturing, 5 (2011) 252-263.

[12] H. Xu, A. Kahraman, N.E. Anderson, D.G. Maddock, Prediction of mechanical efficiency of parallel-axis gear pairs, J MECH DESIGN, 129 (2007) 58-68.

[13] C. Cioc, S. Cioc, L. Moraru, A. Kahraman, T.G. Keith, A Deterministic Elastohydrodynamic Lubrication Model of High-Speed Rotorcraft Transmission Components, TRIBOL T, 45 (2002) 556-562.

[14] Liu, H., et al., Starved lubrication of a spur gear pair. Tribology International, 2016. 94: p. 52-60.

[15] Li, Z., et al., Mesh stiffness and nonlinear dynamic response of a spur gear pair considering tribo-dynamic effect. Mechanism and Machine Theory, 2020. 153: p. 103989.

[16] S. Hou, J. Wei, A. Zhang, T.C. Lim, C. Zhang, Study of Dynamic Model of Helical/Herringbone Planetary Gear System With Friction Excitation, JOURNAL OF COMPUTATIONAL AND NONLINEAR DYNAMICS, 13 (2018).

[17] L. Han, H. Qi, Dynamic response analysis of helical gear pair considering the interaction between friction and mesh stiffness, MECCANICA, 54 (2019) 2325-2337.

[18] D. Yi, X. Zhao, X. Guo, Y. Jiang, C. Wang, X. Lai, X. Huang, L. Chen, [Evaluation of carrying capacity and spatial pattern matching on urban-rural construction land in the Poyang Lake urban agglomeration, China]., Ying yong sheng tai xue bao = The journal of applied ecology, 30 (2019).

[19] J. LIN, R.G. PARKER, Sensitivity of planetary gear natural frequencies and vibration modes to model parameters, J SOUND VIB, 228 (1999) 109-128.

[20] S. LI, A. KAHRAMAN, A Method to Derive Friction and Rolling Power Loss Formulae for Mixed Elastohydrodynamic Lubrication, Journal of Advanced Mechanical Design, Systems, and Manufacturing, 5 (2011) 252-263.

[21] Z. Chen, S. Yan, C. Dawei, H. Peiying, C. Huatai, Y. Jing, Z. Hongxia, Exploration on the spatial spillover effect of infrastructure network on urbanization: A case study in Wuhan urban agglomeration, SUSTAIN CITIES SOC, 47 (2019).

[22] S. Bae, K. Seo, D. Kim, Effect of friction on the contact stress of a coated polymer gear, FRICTION, 8 (2020) 1169-1177.

[23] M. Keller, T. Wimmer, L. Bobach, D. Bartel, TEHL simulation model for the tooth flank contact of a single tooth gearbox under mixed friction conditions, TRIBOL INT, 151 (2020) 106409.

[24] C.I. Park, Tooth friction force and transmission error of spur gears due to sliding friction, J MECH SCI TECHNOL, 33 (2019) 1311-1319.

[25] H. Ma, M. Feng, Z. Li, R. Feng, B. Wen, Time-varying mesh characteristics of a spur gear pair considering the tip-fillet and friction, MECCANICA, 52 (2017) 1695-1709.

[26] S.S. Ghosh, G. Chakraborty, Parametric instability of a multi-degree-of-freedom spur gear system with friction, J SOUND VIB, 354 (2015) 236-253.

Supplementary Files

This is a list of supplementary files associated with this preprint. Click to download.

- Graphicalabstract.pdf
- Highlights.pdf